

**Horizontal-Velocity and Variance Measurements in the
Stable Boundary Layer using Doppler Lidar:
Sensitivity to Averaging Procedures**

YELENA L. PICHUGINA¹, ROBERT M. BANTA², NEIL D. KELLEY³, BONNIE J. JONKMAN,³ SARA C.
TUCKER,¹ ROB K. NEWSOM,⁴ AND W. ALAN BREWER²

- 1 Cooperative Institute for Research in Environmental Sciences (CIRES) Boulder, Colorado
- 2 Earth System Research Laboratory (ESRL), NOAA, Boulder, Colorado
- 3 National Renewable Energy Laboratory, Golden, Colorado
- 4 Pacific Northwest National Laboratories, Richland, Washington

Corresponding Author Address:

Yelena L. Pichugina

NOAA/CSD3
325 Broadway
Boulder CO 80305
Ph. 303-497-6863

E-mail: yelena.pichugina@noaa.gov

31-Mar-08

Abstract

Quantitative data on turbulence variables aloft – above the region of the atmosphere conveniently measured from towers – has been an important but difficult measurement need for advancing understanding and modeling of the stable boundary layer (SBL). Vertical profiles of streamwise velocity variances obtained from NOAA’s High Resolution Doppler Lidar (HRDL), which have been shown to be approximately equal to turbulence kinetic energy (TKE) for stable conditions, are a measure of the turbulence in the SBL. In the present study, the mean horizontal wind component U and variance σ_u^2 were computed from HRDL measurements of the line-of-sight (LOS) velocity using a method described by Banta et al. (2002), which uses an elevation (vertical-slice) scanning technique. The method was tested on datasets obtained during the Lamar Low-Level Jet Project (LLLJP) carried out in early September 2003, near the town of Lamar in southeastern Colorado.

This paper compares U with mean wind speed obtained from sodar and sonic anemometer measurements. The results for the mean U and mean wind speed measured by sodar and in-situ instruments for all nights of LLLJP show high correlation (0.71-0.97), independent of sampling strategies and averaging procedures, and correlation coefficients consistently > 0.9 for four high-wind nights, when the low-level jet speeds exceeded 15 m s^{-1} at some time during the night. Comparison of estimates of variance, on the other hand, proved sensitive to both the spatial and temporal averaging parameters. Several series of averaging tests are described, to find the best correlation between TKE calculated from sonic anemometer data at several tower levels and lidar measurements of horizontal velocity variance σ_u^2 . Because of the nonstationarity of the SBL data, best results were obtained when the velocity data were first averaged over intervals

of 1 min, and then further averaged over three to 15 consecutive 1-min intervals, with best results for the 10 and 15-min averaging periods. For these cases, correlation coefficients exceeded 0.9.

As a part of the analysis, Eulerian integral time scales (τ) were estimated for the four high-wind nights. Time series of τ through each night indicated erratic behavior consistent with the nonstationarity. Histograms of τ showed a mode at 4-5 s, but frequent occurrences of larger τ values, mostly between 10 and 100 s.

1. Introduction

Recent emphasis on the stable boundary layer (SBL) has reflected its importance to a number of applications, including atmospheric transport and diffusion, air quality, emergency response, wind energy, and many more, as well as the crucial problem of representing SBL processes in numerical weather prediction (NWP) models. A limitation has been the ability to obtain reliable high-resolution profile measurements of mean and especially turbulence quantities above the layer routinely sampled by in-situ instruments on meteorological towers. Mean and turbulent fields in the SBL are most often inhomogeneous and nonstationary, and averaging procedures developed for stationary time series have been demonstrated to be mostly unreliable under stable conditions (Vickers and Mahrt 2003, 2005; Mahrt and Vickers 2006). Therefore, progress in understanding the SBL has been slower than its unstable and neutral counterparts.

The important tradeoff for investigating turbulence in the stable boundary layer has been to obtain the statistics of fluctuating quantities, including variances, covariances, and the higher-order moments, over time intervals long enough to achieve statistical reliability, but short enough to be unaffected by the nonstationarity. If the time periods of significant variability are sufficiently short, it may be impossible to sample in a meaningful way. In this study we address the strong-wind, weakly stable boundary layer (wSBL). The hope would be that in this case, reasonable periods of acceptably stationary behavior might be definable. The speed of the low-level jet (LLJ), which drives the dynamics of this boundary layer (Banta et al. 2006), has been observed to vary slowly in time or even remain constant on some nights, and its mean properties have been observed to be constant over areas of a few 10's to a few hundred kilometers across (Banta et al. 2002; Song et al. 2005). Flow properties in the subject layer, however, often exhibit

significant nonstationarity, raising questions about how to sample this layer and whether meaningful turbulence statistics can even be calculated from lidar or tower data.

Remote-sensing techniques using Doppler lidar to measure mean-wind and velocity-variance profiles have been used to study the SBL. A technique for the calculation of both the mean horizontal velocity component aligned with the prevalent wind flow (streamwise velocity U) and the streamwise variance σ_u^2 using elevation or vertical-slice scans, was proposed by Banta et al. (2002, 2006). The statistics are computed within horizontal layers of specified depth (bin size hereafter). In the present study, we apply this technique to scan data obtained during the Lamar Low-Level Jet Project (LLLJP) carried out in early September 2003, near the town of Lamar in southeastern Colorado. Analysis of the data showed that the magnitude and shape of the *mean* wind profiles were largely insensitive to the averaging procedure, but the *variance* profiles were sensitive to the time-averaging procedures and also somewhat sensitive to the vertical binning.

This approach has the advantage of subjecting data to a spatial averaging across the scan before the temporal averaging, offering the possibility of reducing the time needed for a steady, statistically significant variance estimate, and thus addressing the stationarity problem. The question to be addressed in this study is, can useful values of these quantities be obtained in the nocturnal SBL despite the significant limitations imposed by the temporal variability of the flow, including turbulence? The purpose of the study is to determine whether appropriate averaging parameters can be selected, so that this technique can be used under weakly stable conditions to estimate profiles of turbulence kinetic energy (TKE), an important quantity in the SBL, in the region within and above that normally accessible to tower measurements. During the LLLJP we were fortunate to have available simultaneous data from four levels on a 120-m meteorological

tower and a Doppler sodar. Here we present intercomparisons of the Doppler lidar technique with sonic anemometer measurements on the 120-m tower and with mean wind profile data from the sodar.

The paper is organized as follows: Section 2 describes the instrumentation and measurements from the experiment, and HRDL data processing procedures. Section 3 presents the results of the streamwise velocity and variance calculations over a range of averaging time scale and vertical-bin sizes and compares HRDL data against in-situ and sodar measurements. The sensitivity of streamwise velocity variance to both spatial and temporal averaging is addressed by regression analysis of lidar streamwise variances and turbulent kinetic energy (TKE) calculated from sonic anemometer data. Section 4 summarizes the results and draws conclusions.

2. Instrumentation and measurements

a. The Lamar Low-Level Jet Program (LLLJP)

During 2001-2003 U.S. Department of Energy (DOE) National Renewable Energy Laboratory (NREL) and General Electric (GE) initiated a program to study mean and turbulent wind characteristics at a site about 20 miles south of the town Lamar, Colorado (Kelley et al. 2004; Pichugina et al. 2004, 2005). Called the Lamar Low-Level Jet Program (LLLJP), it was situated on a plateau south of the Arkansas River Basin. Locally, the terrain is relatively flat and homogenous, but with more complex elements to the west and north. The instrumentation in this campaign included sonic anemometers at four levels on a 120-m meteorological tower, an acoustic wind profiler, and, during September 2003, HRDL.

1) TOWER AND SODAR

A 120-m tall meteorological tower was installed at the LLLJP site by General Electric Wind Energy (GE Wind). The geographical coordinates of the tower were 37.6683° N and 102.66375° W. Its base was at an elevation of 1357 m above mean sea level. NREL instrumented the tower with three-axis sonic anemometers (Applied Technologies, Model SAT/3K) mounted at heights of 54, 67, 85, and 116 m AGL, to provide three-component wind and virtual temperature data at a sampling rate of 20 Hz on all data channels from 1600 to 0800 local standard time (2300-1500 UTC). The high-resolution sonic data were collected and processed by NREL continuously from March 2002 through April 2003 and again briefly during 1-16 September 2003. Means and variances were calculated over 1-, 5-, and 10-min intervals, except for the last analysis, in which data were first averaged over 1-min intervals, and then the 1-min means and variances were further averaged over 3-, 5-, 10-, and 15-min blocks, as in Banta et al. (2003).

An acoustic wind profiler (sodar) was also operated at this site starting in May 2002. This Scintec Model MFAS mid-range sodar had a vertical measurement range from 40 to 500 m. It provided profiles of the horizontal wind speed and direction, or the north-south, east-west, and vertical velocity components at 10-m vertical resolution. Data were averaged over 10-min intervals, with a published precision of 0.3 m s⁻¹. This instrument employs a phased-array antenna that can provide nine electronically steerable beams emitting up to 10 frequencies. The antenna is installed within an octagonal acoustic enclosure designed to reduce environmental noise at the antenna itself. The antenna was located 109 m southeast of the tower base at the same elevation. This location was chosen to be as close as possible to the tower to obtain a better comparison of sodar derived winds with those directly measured by instruments on the tower.

A confidence factor (which ranges from 0 to 5) is determined for the sodar data from an aggregate of three criteria, which are based on the degree of consistency of the individual results from each of the 10 transmitted frequencies, the returned signal strength, and the level of consistency between vertical layers (range gates). Values of 3 or more are generally associated with reasonable estimates of the wind velocity.

Detailed descriptions of the LLLJP, sodar and tower observations over about a 1½-year period can be found in Kelley et al. (2004). In a recent study comparing mean tower, sodar, and HRDL velocity measurements, Kelley et al. (2007) found that velocity-induced systematic differences arise from the distorted flow field in the vicinity of the sonic anemometers created by Reynolds number effects in the air flow around the cylindrical apex legs of the lattice tower structure. These differences can range from indicated overspeeds of 50% or 2 m s^{-1} at low wind speeds (4 m s^{-1}) to underspeeds of 9% or 2 m s^{-1} at 22 m s^{-1} . Very little difference was seen at velocities near 10 m s^{-1} . Thus, such effects on the sonic measurements will also influence the lidar-sonic intercomparisons to be presented.

The National Oceanic and Atmospheric Administration's Earth System Research Laboratory (NOAA/ESRL) joined the program for two weeks in September 2003 and deployed the High Resolution Doppler Lidar (HRDL) to the site, at the same elevation as the tower and sodar with coordinates 37.6657° N and 102.6668° W . Description of the HRDL data set and some results can be found in Pichugina et al. (2004, 2005), and Banta et al. (2006).

2) HRDL DESCRIPTION

NOAA's High Resolution Doppler Lidar (HRDL) is a scanning, active remote sensing system that measures range-resolved profiles of Doppler velocity and aerosol backscatter (Grund et al., 2001, Wulfmeyer et al. 2000). The lidar operated with a pulse repetition frequency (PRF)

of 200 Hz, typically averaging results from 100 pulses to form range-resolved, line-of-sight (LOS) velocity estimates twice per second with a range resolution of 30 m, which matches the 200-ns pulse width. Detailed descriptions of HRDL operating characteristics for another nighttime measurement campaign, the Cooperative Surface-Atmosphere Exchange Study (CASES-99) can be found in Banta et al. (2002) and Newsom and Banta (2003).

HRDL data were collected for eleven nights from local sunset (0000 UTC) until prior to sunrise (usually 1000-1100 UTC) by performing a variety of different scans (conical, vertical-slice, and staring) to address different scanning objectives. Most of the time HRDL was operated in an elevation-angle scanning mode (vertical-slice scans). Occasionally, during the night HRDL also performed stare “scans,” when the lidar beam was held fixed at an azimuth angle parallel to the mean horizontal wind direction, usually at an elevation angle of 10°. The present paper will focus on analysis of data from vertical-slice scans, which accounted for 70-75% of the operational time. These scans have also proven to be effective in the analysis of the near-neutral surface-layer structure (Drobinski et al. 2004), velocity field and atmospheric TKE dissipation (Smalikho et al., 2005), shear-instability, Kelvin-Helmholtz type waves (Newsom and Banta, 2002, Blumen et al. 2001), and low-level jet evolution (Banta et al., 2002, 2003, 2006, 2007).

b. Averaging procedures

1) TEMPORAL AVERAGING

A formal approach to determining the length of time required for a statistically significant average of second and higher-order moments was described by Lenschow et al. (1994). The required averaging period is a function of the integral time scale τ and the desired

accuracy (e.g., 10%). For a second moment and 10% accuracy an averaging interval of about 250τ is required. However, Lenschow et al. repeatedly caution that this formalism only applies to stationary time series. Their examples are for unstable conditions, for which nearly stationary periods in the time series can be identified or constructed (e.g., by filtering). In our stable case studies, however, the turbulence in the subjet layer was nonstationary. Even calculating steady values for τ was challenging.

Because the hope was that periods of reasonable stationarity could be found for sampling purposes, we attempted to apply the Lenschow et al. (1994) technique to our datasets, despite the nonstationarity of the data. The results of this attempt are presented in Appendix A. Briefly, we tried several methods of calculation for τ , and the τ time series showed that the values jumped around considerably. Histograms indicated a mode in the distribution at 4-5 s, but frequent occurrences of larger values mostly in the 10-100 s range. Using 5 s as a representative τ value, the Lenschow et al. (1994) procedure requires an averaging period of ~ 20 min for a 10% standard error of the variance estimate. Such periods of steady τ were rare in the dataset. An analysis of one such period is given in Appendix A. The results were about the same as those presented later in this paper for periods when τ behavior was more erratic. Thus, little advantage was evident to restricting the analysis to the “well-behaved” periods.

Alternative approaches for analysis of time series have been developed by Vickers and Mahrt (2003, 2005), who point out that in the stable surface layer, the use of constant averaging intervals, even as short as a minute, routinely produces erratic results because of inadvertent inclusion of more random mesoscale motions as part of the perturbation flow. They developed a method for averaging over shorter intervals of variable width based on the multiresolution heat-flux cospectrum. They further average these short interval values over a one-hour period, to

reduce random flux sampling errors. Fluxes calculated in this way were well behaved except for the most strongly nonstationary records. The fluxes vary smoothly in time and with scale, and show a more systematic relationship to the local gradients. This approach was successfully applied to studies of the very stable boundary layer (Mahrt and Vickers 2006, Banta et al. 2007).

The SBL in the present study more resembles the Mahrt-Vickers conditions. Therefore, one of our approaches will be to calculate the variances over a smaller interval of 1 min, then further average over longer intervals of 3 to 15 min, as previously described in Banta et al. (2003).

2) LIDAR TURBULENCE ESTIMATES

Techniques for calculating vertical profiles of turbulence quantities from lidar active remote-sensing measurements have been described in the literature for velocity statistics, spectra, and TKE dissipation, for unstable and near-neutral BLs. Vertically pointing Doppler lidar data have been used to determine vertical-velocity w statistics, including the variance, third and fourth moments, structure functions, and integral length scales (Lenschow et al. 2000, Lothon and Lenschow 2006). The calculation of dissipation and spectra has used both staring and scanning methods (e.g., Frehlich et al. 1998; Drobinski et al. 2000; Davies et al. 2004; Smalikho et al. 2005).

Methods using full 360° conical azimuth scans to calculate the mean wind, TKE, momentum flux, and certain third-order moments were developed for scanning Doppler radar (Browning and Wexler 1968; Wilson 1970; Orr 1990). The analysis scheme, called the velocity-azimuth display (VAD) technique (Browning and Wexler 1968), can be used for individual conical scans (Browning and Wexler 1968) or for all scans accumulated over a given time interval (Banta et al. 2002). Kropfli (1986) showed that these procedures produced reasonable

estimates of TKE and momentum flux, when compared with tower sonic-anemometer data. Eberhard et al. (1989) applied these techniques to Doppler lidar scan data to investigate a strongly wind-driven unstable daytime boundary layer, and Banta et al. (1997) showed that Doppler lidar could be used to investigate weaker-wind convective boundary layers, if scans were averaged over 20 min or more to achieve statistically well behaved results. Gal-Chen et al. (1992) developed a method for calculating turbulence and flux quantities using scans in elevation at two azimuth angles, one along wind and the other across the wind. Where verification data were available, calculations of turbulence quantities for all these studies, which were in unstable or near-neutral conditions where the shear was small, showed reasonable agreement.

In stable atmospheric conditions, Frisch et al. (1992) used these conical-scanning VAD procedures with cloud-radar data to document the evolution of a nocturnal LLJ in the northern U.S. Great Plains. Values of the quantities were reasonable, although no verification data for the turbulence profiles were provided.

In the present study we describe a different approach to calculating velocity variances, an approach that uses elevation scanning similar to the Gal-Chen method. But rather than full 180° horizon-to-horizon elevation scans, this technique uses repeated sector scans, which were oriented with the scan baseline parallel to the mean horizontal wind direction, over more limited elevation angles (Fig. 1). For this study, the highest elevation angles were typically 8-20 °, scanning usually at a rate of 1° s⁻¹. These scans (which have sometimes been referred to in radar jargon as “range-height indicator” or “RHI” scans) produce a vertical cross section or vertical slice of data from the atmosphere. The data-gathering procedure was to perform a sequence of 360° conical scans at several fixed elevation angles, which took ~5 min, approximately every 20-30 min to determine the mean wind direction. Repeated along-wind vertical-slice scans, which

individually took about 30 s or less to complete, were then performed for periods of 15-30 min or more. During the Lamar project, the wind direction could also be monitored between the conical lidar scan sequences by using the 10-min averaged wind profiles from a Doppler sodar. The analysis procedures will be described in the next section.

3) PROCESSING—VERTICAL BINNING TECHNIQUE

The horizontal wind component (u_h) was estimated by dividing each line-of-sight (LOS) velocity measurement by the cosine of the elevation angle. Thus, u_h represents the horizontal velocity component parallel to the plane of the elevation scan. We assumed that each lidar data point represented an average within the 30-m-long sampling volume (“range gate”) that could be attributed to a point at the centroid of the volume. Estimates of the mean u_h and variance were obtained by first sorting the horizontal wind component results from individual vertical-slice scans into height bins (Fig. 1) and then calculating an average and variance from the u_h data found within each bin. Temporal averaging was accomplished by collecting u_h data from all scans in the averaging period into the height bins prior to averaging.

Variance estimates are particularly sensitive to measurement noise and spurious signals due to hard target returns. Prior to the computation of the mean and variance profiles, radial-velocity estimates were subjected to a quality control procedure to remove obvious outliers from the data. The procedure consisted of detecting large spikes in the SNR (backscatter) field that coincided with radial velocity samples falling within $\pm 0.5 \text{ m s}^{-1}$. These samples were flagged as missing, as they were likely due to hard-target returns. Radial velocities corresponding to weak signal returns were also flagged missing. In addition to these steps, the calculation of the variance was performed by first computing a histogram of the distribution of u_h estimates within a given height bin. The variance for that height bin was then computed using samples falling

within $\pm 5 \text{ m s}^{-1}$ of the mode of the distribution. The 5 m s^{-1} threshold proved appropriate for the CASES-99 and LLLJP SBL datasets, but for conditions with more intense atmospheric turbulence, a larger value may be more appropriate.

Since the scans were aligned along the mean wind direction (at least below the LLJ nose), these estimates represented the mean streamwise wind speed U and the streamwise variance σ_u^2 averaged spatially over each bin and temporally over each averaging interval. Banta et al. (2002) used this technique to produce time-height cross sections of σ_u^2 in the nocturnal SBL, and Drobinski et al. (2004) found reasonable agreement between the HRDL variances and tower-measured streamwise variances in the low-shear, weakly unstable to near-neutral BL during an evening transition.

The lidar-measured horizontal-velocity variance calculated in this way includes many contributions in addition to the desired atmospheric fluctuations represented by σ_u^2 . These include instrumental noise, which will be discussed in the next section, and a variety of sampling issues, including pulse-volume filtering by the lidar, tilt or other horizontal variations of the flow across the horizontally-oriented bins, the existence of vertical shear across the depth of the bin, and others. Each of these effects produces an additive contribution to the variance estimated from the lidar data, which, if large enough, could overwhelm the atmospheric σ_u^2 value being sought. These pure lidar-sampling contributions would be completely uncorrelated with measurements from any other instrument, such as sonic anemometers. In particular, when performing regression analysis between lidar and sonic estimates of σ_u^2 , such instrument-specific sampling effects would act only to degrade the correlations.

To investigate the sensitivity of this procedure to spatial and temporal scales, we computed the mean u_h (U) and its variance σ_u^2 by averaging over several different vertical bin

sizes (1-, 5-, 10-, and 15-m) and by further averaging over data from multiple scans at longer time intervals (1-, 5-, 10-, and 15-min). Initially the mean values agreed well for all averaging parameters, whereas the variances for lidar bins depths of 5 m or more were too large by a factor of 2-3 (Banta et al. 2006). But reducing the bin depth to 1 m produced good agreement between tower and HRDL variances, as reported by Banta et al. (2006). This suggested that the large vertical SBL shear in the mean wind across the bins could be a major contributor to the excessive variances for the larger bins sizes. To account for this factor, the mean shear was removed from the data in each bin before the variance calculation. The velocity difference in the shear calculation was taken as a centered difference across each bin, using data from the adjacent bins above and below. The wind-speed profile in the subject layer was observed to be nearly linear for this dataset, so errors introduced by calculating shear in this way would be small.

4) UNCORRELATED INSTRUMENT NOISE

Techniques to determine the precision of LOS velocity measurements have been previously studied and described by many authors (Rye and Hardesty 1993; Mayor et al. 1997; Frehlich 2001; 2004, Smalikho 2003; Newsom and Banta 2004). We refer the reader to these references for further discussion of measurement precision. Here the measurement error, or “uncorrelated instrument noise,” was estimated by analyzing fixed-beam scans. LOS velocity data were quality controlled as described in the previous section.

The precision of LOS estimates from HRDL, derived from time series analysis of staring data taken during the CASES-99 experiment, is described by Newsom and Banta (2004). They showed that the measurement error varies smoothly with range and is routinely less than 50 cm s^{-1} for ranges less than 1800 m for their late-afternoon study. A similar analysis of the Lamar data show the measurement error was of similar magnitude for ranges less than 1500 m, increasing

rapidly beyond this range due to weakening backscattered signal. It is unclear whether the reduction in maximum range for a given precision was due to a decrease in the lidar sensitivity between the two experiments, or to a difference in the number and/or size of aerosol particles at the different locations. In either case, the correlation between reduction in return signal strength and minimum precision holds, as described in Rye and Hardesty (1993). In our analysis, data were excluded for ranges greater than 1500 m and for ranges less than the HRDL minimum range of 190 m.

Typical estimates of LOS velocity variance due to uncorrelated instrumental noise varied from $0.04 \text{ m}^2 \text{ s}^{-2}$ to $0.25 \text{ m}^2 \text{ s}^{-2}$ (for 100-pulse averaging and 10 sample points per 30-m range gate) in good agreement with the theoretical Cramer-Rao Lower Bound on velocity precision for this instrument, at the corresponding signal-to-noise-ratio (SNR). The uncorrelated noise was therefore attributed to instrument noise. Due to variations in aerosol concentration, the instrument noise for a given range varied night to night, and sometimes even during a night. However, for ranges of $<1500 \text{ m}$ the instrument-noise contribution to the measured variance typically had values of 0.04 to $0.06 \text{ m}^2 \text{ s}^{-2}$. These values compare with typical low-end measured atmospheric velocity-variance values of greater than $0.2 \text{ m}^2 \text{ s}^{-2}$ (most were greater than $0.5 \text{ m}^2 \text{ s}^{-2}$), which will be presented in Section 3. An example of such relationships is shown in Fig. 2. Thus, in most situations, the instrument-dependent uncertainty on the velocity estimates is a small fraction of the total measured velocity variance, except near the top of the SBL, where atmospheric turbulence becomes small. For a straightforward but conservative correction, a noise value of $0.05 \text{ m}^2 \text{ s}^{-2}$ was subtracted from the total measured variance to estimate atmospheric velocity variance. Procedures for more careful extraction of the instrument noise variance from the total variance on a scan by scan basis are currently under development but

preliminary studies have shown that subtracting $0.05 \text{ m}^2 \text{ s}^{-2}$ to account for the instrument noise at each altitude introduces less than $\pm 10 \text{ cm s}^{-1}$ of measurement error into the final atmospheric variance estimate.

d. Current dataset

Data for this study were obtained from the four LLLJP nights used in the Banta et al. (2006) study (5, 6, 9, and 15 September 2003), when the LLJ speed exceeded 15 m s^{-1} at some time during the night. On these strong-wind nights the flow was weakly stable. The velocity profile generally was linear from the top of the surface layer (lowest 10% of the subjet layer) to just below the LLJ nose (generally 150-250 m AGL), implying that the wind-speed shear was constant through this layer. Bulk Richardson numbers, which were calculated from differences in U and θ between the 54- and 85-m tower levels within the subjet layer, were less than 0.2 and mostly ~ 0.1 . For the strong LLJ cases of this dataset, directional shear was also negligible through this layer.

An aspect of the variance comparisons is that the lidar technique measures the streamwise variance, whereas the quantity of greatest interest is TKE. Banta et al. (2006) have presented evidence (including data from previous studies in the literature) that for stable conditions, σ_u^2 is proportional to TKE, and the proportionality constant is approximately equal to 1. A direct comparison of these quantities using tower data from the current LLLJP dataset (Fig. 3) also shows excellent agreement, with correlation coefficients of 0.98 (Table 1). This near equivalence was attributed to the anisotropy of the turbulence, with σ_u^2 being the largest component, combined with the factor of $1/2$ in the definition of TKE (Banta et al. 2006). In this study we compare HRDL-measured σ_u^2 first with tower-measured σ_u^2 and then with TKE.

One of the goals of this paper was to determine whether useful profiles of σ_u^2 are obtainable in spite of lack of stationarity and the significant differences in sampling between the two measurement systems. Because the HRDL streamwise-velocity variance proved to be sensitive to both spatial and temporal averaging procedures, an important aspect of this investigation was to determine the best value for the vertical bins and time intervals, to optimize the agreement with the in-situ measurements. An even more basic issue is the accuracy of either lidar or sonic variance estimates. Contributions to the uncertainty in estimates of σ_u^2 based on lidar data have been discussed, but uncertainties in the sonic estimates are also introduced, for example, by flow distortion by the tower on the sonic anemometer measurements and whether the averaging interval was sufficiently long to obtain meaningful variance values. Further issues arise when comparing HRDL-derived data with data from other instruments. Comparing HRDL variances with those derived from sonic anemometers, as presented later in this study, involves spatial variations in turbulence between measurement locations, stationarity of the flow and turbulence for the averaging period of the anemometer time series, and differences between the spatial averaging procedure used for the HRDL estimates and the temporal averaging used for the sonic estimates. Each of these effects, if significant, will reduce the correlation between lidar and sonic variances. For these and many other reasons, comparisons between tower and lidar variances were not expected to be well correlated, but we proceeded with the analysis.

3. Results

Before comparing variance values, we first assess how well HRDL estimates of the mean wind agree with sodar and sonic anemometer estimates.

a. HRDL vs sodar: Mean wind

Profiles of the horizontal wind speed from the sodar at the Lamar site were available in 10-min time intervals and 10-m vertical increments, as described above, and we used these to compare with the lidar measurements. An example of 10-min lidar streamwise velocity profiles (blue) and 10-min wind-speed profiles computed from sodar observations (red) are shown in Fig. 4a for every hour from 0130 to 0930 UTC during the night of September 15. Profiles of all available sodar data (shown by red dots) are overlapped by red pluses that represent sodar data obtained with confidence factor equal or greater than 3.

These representative profiles show good agreement up to approximately the height of the first LLJ maximum, then differences in profile shape above that height. They also show that choosing the confidence-factor threshold of 3 seems to do a reasonable job of identifying the good sodar velocities. For the entire LLLJP dataset, profiles from both instruments also generally showed good agreement up to near the jet nose, which was often 150-250 m AGL, when the sodar confidence factor was 3 or more. Above this height the profiles diverge, with the sodar tending to read stronger velocities than the lidar (sometimes even when the confidence factor was high). The sodar data also tended to drop out during the sunset and sunrise transitions, as has been reported by other researchers (Maughan et al. 1982, Emeis et al. 2004).

A scatter plot of 10-min, 10-m lidar U and sodar wind speed, obtained for the night of 15 September, is shown in Fig. 4b. The best fit to the data is shown as a solid line with correlation coefficient of 0.94 as shown in Table 1 along with the bias and slope of the line of best fit. As in Fig. 4a, all available sodar data are shown by dots, with plus signs representing sodar data obtained with confidence factor equal or greater than 3. Because we have only 10-min, 10-m sodar data, these are the only comparisons made. We only note that for the rest of the nights

with long enough data sets (more than 5-6 hours of corresponding data), the correlation between the two remote sensing estimates—HRDL streamwise velocities and sodar wind speeds—was also very high with correlation coefficients greater than 0.9 for nearly all of the periods studied. Since the sodar signal was strong in the layer below the jet nose (tending to weaken significantly above), the high correlations imply that both sodar and lidar were producing good estimates of the wind speed in the region below the top of the SBL, which generally coincided with the LLJ nose.

b. Mean wind speed: HRDL vs sonic

The accuracy of the mean streamwise velocity was also examined by comparing it against wind speed measured by sonic anemometers mounted on the 120-m tower, which was 167 m away from the lidar. An example of a time-height cross section of HRDL streamwise velocity for the night of 5 September is shown in Fig. 5 (top panel), where each colored vertical data line represents a vertical profile of the streamwise mean velocity computed in 1-m bins. The bottom panel of the figure shows a time series of sonic wind speed at four levels (solid line) overlapped by lidar data (shown by plus signs) calculated at the heights of the sonic measurements, as indicated by dotted lines in the top panel. Both lidar and sonic anemometer data were averaged over 1-min time intervals. The plus signs are mostly indistinguishable from the lines in the bottom plot, indicating good agreement between both instruments in the evolution of the mean and fluctuating motions for each height, which was typical of all nights studied. On this night LLJ speeds peaked at ~ 0400 UTC and gradually declined through the night, which is also evident in the tower measurements.

Scatter plots of wind speed from sonic anemometers at four tower levels and HRDL-measured streamwise velocity computed at the heights of sonic measurements for the night of 5 September are shown in Fig. 6. In the left panel data from both instruments were averaged over 1-min and streamwise velocities were computed within 1-m vertical bins; and in the right panel data were averaged over 10-min and streamwise velocities were computed within 10-m vertical bins. Both plots show good agreement between lidar and sonic anemometer measurements, with correlation coefficients of 0.95-0.98 for all four heights as listed in Table 1, along with the slope and bias of the best-fit lines.

However, the agreement between lidar and sonic anemometer measurements varied significantly between nights. During some nights, different correlation statistics were obtained for each level. An example of the agreement in the HRDL and sonic anemometer measurements of the mean wind is shown in Table 2, where both data sets were averaged over 1-min time interval, and HRDL data binned into 1-m vertical layers. The first column in the table lists the date during LLLJP and the other columns show correlation coefficients obtained for the heights of the in-situ instruments.

The better correlations (greater than 0.9) were observed for 5, 6, 9, 10, and 15 September, when the overnight mean wind was greater than 15 m s^{-1} (“high-wind” nights as in Banta et al., 2002). The lower correlation observed for the nights of 3 and 12 September were due partially to different atmospheric conditions, when wind speeds remained below $7\text{-}8 \text{ m s}^{-1}$, and partially to small sample sizes such as for the night of 3 September, when HRDL measurements were obtained only for 3 h from 0430 to 0740 UTC. Decreases in the agreement of the wind speed measured by sonic anemometers and mean streamwise velocity from HRDL measurements for “low-“ or “low-moderate-wind” nights, when wind speeds remained below $7\text{-}8 \text{ m s}^{-1}$, could be

explained by greater influence of horizontal variability, including terrain effects, and flow nonstationarity, which were observed in the lidar scans at the lower wind speeds. For the lower-wind cases, difficulties in estimation of prevalent wind direction, existence of directional shear in the vertical (not observed at the higher wind speeds), and positioning the lidar beam precisely along the mainstream wind also probably contributed to lower correlation values.

Averaging sonic and HRDL data over different time intervals of 1-, 5-, 10-, and 15- min, or computing streamwise velocity within different (1-, 5-, 10-, 15-m) vertical bins did not produce a significant change in agreement between both data sets for the night of 5 September, showing high correlation coefficients for all tests (0.94-0.96). Similar analysis for all LLLJP nights shows that these results were typical: mean speeds between the lidar and sonic anemometer measurements were well correlated, especially for the stronger-wind nights, independent of sampling strategies and averaging procedures.

c. Velocity variance HRDL vs sonic

Unlike the mean wind speeds, the streamwise velocity variance estimates proved sensitive to both temporal averaging interval and depth of vertical bins; for example, they could differ by nearly 50% as the vertical bin size was increased from 1 m to 10 m, as illustrated in Fig. 7. This value is less than the factor of 2-3 reported by Banta et al. (2006), because the mean shear contribution (as well as the “instrument noise”) has been removed from the data in Fig. 7. This figure shows sample profiles of 5-min U (left) and σ_u^2 (right) calculated by averaging within 1-, 5-, and 10-m vertical bins. Variance differences among the various bin sizes are larger here for heights within the high-shear zone below the LLJ and smaller above the jet-speed maximum, where the shear and variance values were smaller.

Fig. 8 shows the time-height cross section of HRDL streamwise velocity variance for 5 September (which accompanies the mean-wind plot in Fig. 5a), for 1-m (upper) and 10-m (lower) vertical binning. In the upper panel, stronger turbulence at the higher levels indicates an upside-down turbulence structure as described in Mahrt and Vickers (2002) and Banta et al. (2002). The figure illustrates an increase of variances by as much as 50% for the larger bin size, as shown in Fig. 7, for the entire nighttime period. The differences appear most significant in the atmospheric layer of 10-150 m. Since the mean shear contribution has been removed in the calculation of the variance, other undetermined factors are responsible for this discrepancy.

An example of a time-height cross section of σ_u^2 for the night of 15 September is shown in Fig. 9 (top panel), averaged over 1-min and calculated in 1-m bins, and several time-series of tower-measured TKE (bottom) also averaged over 1-min. Both instruments show good agreement in the evolution of turbulence through the night. A period of low turbulence during the evening transition period from 0130 to 0230 UTC evolved into a period of increased turbulence (0230-0600 UTC). Both instruments show a maximum of the turbulence early in the local morning (0100-0300 MST or 0800-1000 UTC). The profiles and time series in these plots have not been subjected to any explicit additional smoothing in time or in the vertical, other than that inherent in the binning process and in the lidar pulse-volume averaging. So overall this figure shows that successive lidar variance profiles exhibit continuity in time, and that the trends in the 1-min variance-TKE data from both instruments agree at least semi-quantitatively, despite the short averaging periods.

Scatter diagrams showing comparisons between HRDL- and tower-measured σ_u^2 are shown in Fig. 10. The six panels of this figure represent data from both instruments averaged over (left column) 5 min and (right column) 10 min. The streamwise σ_u^2 are calculated within

vertical bins of 1 m (top row), 5 m, and 10 m. The effects of vertical bin size for this sample were negligible, as can be seen in Table 1. Although the correlation coefficients for 1- and 10-m binning are similar, 10-m bins produced larger negative biases.

The effect of temporal averaging is also shown in Table 1. The smaller correlations for 1-min averaging increase as expected for 5-min averaging to values of ~ 0.85 , due to the larger sample size. For 10-min intervals, the correlations decrease slightly, possibly as a result of nonstationary effects. A noteworthy aspect of the scatter diagrams in Fig. 10 is the behavior at low turbulence values, when the tower-measured variances were $\leq 0.2 \text{ m}^2 \text{ s}^{-2}$. Such weak turbulence is often associated with low wind speeds, and /or transition periods, conditions that were also shown to degrade the correlations in the mean-wind intercomparisons. Here HRDL variances are systematically much larger than the tower variances. Inspection of individual lidar scans (such as Fig. 1) indicated greater spatial variability along the scan at lower turbulence and wind speeds, in contrast to higher-wind cross sections, which were characteristically more horizontally stratified. The greater horizontal variability combined with weaker winds may account for much of the discrepancy in variances at the lower wind speeds. Other effects mentioned in Section 3b, such as spatial and temporal directional variability for the weaker-flow cases, would also contribute here. The fact that the correlation was rather poor for this grouping of points means that the variances at higher wind speeds were even more highly correlated than the r 's presented in Table 1 (for all data points) would indicate.

As described in Section 2d, the quantity of greatest interest for turbulence applications is TKE rather than σ_u^2 , but the magnitude of TKE was found to be about equal to that of σ_u^2 for stable conditions. The correlation coefficients and biases for tower TKE vs. HRDL streamwise

variance (Table 1) are essentially the same, as should be expected, confirming that TKE and σ_u^2 were nearly interchangeable for these cases.

As a final test we averaged together consecutive 1-min means for 3-, 5-, 10, and 15-min periods for both instruments to roughly emulate the Vickers-Mahrt approach. The results, given in Fig. 11, and Table 1, show that this procedure produced the best fit of all, with correlation coefficients of 0.90 or more for averaging ten or fifteen successive 1-min means. This improvement in correlation is an indication that nonstationary effects contributed to the variance magnitude in the previous examples. The discrepancies at low turbulence values noted in Fig. 10 are also evident in this figure, indicating lower confidence at small σ_u^2 values, but even better correlations for the stronger-turbulence region of the plot than indicated by the r values in Table 1.

4. Conclusion

Obtaining accurate profiles of mean and especially turbulent quantities in atmospheric layers above those conveniently measured by towers is difficult but important for progress in research into the stable boundary layer, which is generally strongly sheared. Within the tower layer it has been shown that special analysis techniques are required to compensate for nonstationary effects under stable conditions. Above the tower layer, it is not known what kind of sampling is required, since stable flow may be inhomogeneous in addition to being nonstationary.

Here we have presented measurements of mean and turbulence quantities in this layer of the atmosphere based on two measurement systems, tower-mounted sonic anemometers and HRDL. Each system has its own instrumental and sampling uncertainties that contribute to the measurement, and then further uncertainties arise from attempting to compare data from two

different instruments, sampling at two different locations, using different analysis procedures. For profiles of mean wind speed (also sampled by Doppler sodar), these differences seem to matter very little, because discrepancies between the measured profiles were small, independent of averaging parameters. For turbulent velocity variance profiles, however, it is another matter. We initially expected poor correlations between the datasets, because individually or collectively, the effect of all these independent uncertainties should have been to obscure the atmospheric contribution to the variances.

The resulting correlations between the sonic-measured and lidar-measured variances were sensitive to the manner in which the calculations were performed. But when appropriate procedures were chosen, which accounted for the nonstationarity of the flow and the strength of the vertical variations, correlation coefficients of 0.8-0.9 or more were obtained for the stronger-wind nights, indicating significant agreement. This agreement implies that both systems and procedures were sampling mainly atmospheric variance, because the other sources of variance would be uncorrelated, and also that estimations of this atmospheric variance did not suffer from significant decorrelation as a result of spatial or temporal separation of the measurements. The agreement gives confidence in the results from both instruments, and their corresponding analysis procedures.

In using the Doppler lidar vertical-scanning technique for estimating σ_u^2 we noted in one example that large differences (~50%) could still exist for different averaging parameters (bin sizes, in this example), even though the mean shear was removed from the data. This is an indication that precise averaging parameters are not well known. Additionally, effects that could act to obscure the estimation of atmospheric variance values (horizontal variability or tilt of the flow within bins, other terrain effects, directional shear with height, nonstationarity, etc.), which

were inferred to be negligible in our cases, may be important in other circumstances. These possibilities suggest that it may be important to have an independent measurement of variance values available as a reality check, to be sure the values are at least of appropriate magnitude. In the SBL an alternative check has been suggested by Banta et al. (2006), who found that the maximum value in the streamwise standard deviation (square root of σ_u^2) near the surface is often about 5% of the wind speed at the top of the SBL, which generally coincides with the first LLJ maximum in wind speed above the surface. The LLJ speed is obtainable from Doppler-lidar mean-wind profiles, which this study has demonstrated to be a high-confidence measurement.

Acknowledgments. Field data acquisition and much of the analysis for this research were funded by the National Renewable Energy Research Laboratory (NREL) of the U.S. Department of Energy (DOE) under Interagency Agreement DOE-AI36-03GO13094. Portions of the analysis were also supported by the U.S. Army Research Office (Dr. Walter Bach) of the Army Research Laboratory under Proposal No. 43711-EV, and analysis and manuscript preparation were also supported by the NOAA Air Quality and Health of the Atmosphere Programs. The NREL work was supported by the U.S. Department of Energy under contract No. DE-AC36-99GO10337. We thank our colleagues Scott Sandberg, Janet Machol, Richard Marchbanks, Brandi McCarty, Joanne George, Lisa Darby, Andreas Muschinski, Jennifer Keane, Ann Weickmann, Ron Richter, and Raul Alvarez from ESRL, and the following from NREL: Mari Shirazi, Dave Jager, S. Wilde and J. Adams. We also wish to acknowledge the Emick family, on whose ranch this project took place, and helpful discussions with Larry Mahrt and Lisa Darby.

APPENDIX A

All of our cases were decidedly stable. In clear-sky conditions over the semi-arid Great Plains, this means that strong temperature inversions prevailed each night, even despite the strong winds of our principal study nights presented here. As in the data presented for 15 September by Pichugina et al (2005) and for 5 September by Banta (2008) lapse rates in the subject layer above the surface layer were $\sim 0.03^\circ \text{ m}^{-1}$ (and much larger in the surface layer), and bulk Ri 's were ~ 0.1 , but not smaller. LLJ speeds were observed to be relatively constant or slowly varying (*Lamar ref.??*, Banta 2008), but below the jet, wind speeds and turbulence at a given level exhibited nonstationary behavior throughout each night. For example, Fig. A1a shows a plot of the Eulerian time scale τ vs. time at 54 m height for the night of 9 September. The erratic temporal behavior reflects not only the nonstationarity of the velocity time series, but also the fact that τ is one of the most difficult second-order statistics to obtain a statistically stable estimate of, as alluded to by Lenschow et al. (1994), Panofsky and Dutton (1984), and in the recent discussions of Treviño and Andreas (2006, 2008) and Eckman (2008), even under relatively stationary atmospheric flow conditions, which was not the case for our dataset. Three methods were used to estimate τ , as discussed in Appendix B.

Although the behavior in Fig. A1a strongly suggests that a representative value of τ for the Lenschow et al. (1994) analysis cannot be found, we proceeded formally with the analysis in an attempt at even rough guidance as to appropriate averaging time intervals. The major question is, which value of τ is appropriate? To understand the range of likely values for τ , we plotted distributions of τ for each night and at each tower measurement level. Typical τ distributions are illustrated in Fig. A1b, which shows the histogram for the data shown in Fig. A1a. Additionally, means, medians, and modes of the τ data for each level and each averaging

period for all days and periods considered are given in Table A1. The occurrences of large τ values significantly influenced the mean and median, which were often near 15 and 10 s respectively. But distinct modes at smaller values were evident around 4-5 s. To further check the representativeness of these findings, we plotted the distribution of τ for all nights when HRDL was at Lamar (1-16 September; Fig. A1c), and for all nighttime periods when the tower was operating between March 2002 and March 2003 and also including the 28 August-16 September 2003 period of operation (Fig. A1d). The results are consistent with the behavior observed on the individual nights.

Periods of 30-60 min when τ was nearly constant were rare in the dataset. When they occurred they tended to occur near the end of the early-evening transition between 0300 and 0400 UTC (sunset was ~0100 UTC). τ values during these periods were ~ 5 s, i.e., represented consecutive periods when τ was near its mode value. The required averaging period of 250τ , which would be ~20 min, would be met for these periods. Plots of tower-measured TKE vs. HRDL streamwise variance for one such period on 15 September are shown in Fig. A2. The lidar variances were averaged in 1-min blocks which in turn were further averaged into intervals of 3 to 15 min. As described in Section 3c, this was the method that produced the best agreement with the tower measurements. Correlation coefficients were 0.8 to 0.9, consistent with analyses presented in the text based on all time periods, not just when τ was well behaved. The other regression parameters for this analysis were similar to the corresponding ones at the bottom of Table 1. The overall conclusion here is that the agreement between tower- and HRDL-measured variances during periods when τ was well behaved was good but no better than during the other periods analyzed.

APPENDIX B

Eulerian integral scales τ for the nights of 1-16 Sept were estimated using three different techniques. The techniques were (1) integrating the autocorrelation function of 10-min streamwise velocities (with 10-min mean removed) over positive lags up to the first zero crossing, (2) calculating the peak 30-min spectra, $f S(f)$, and dividing the period by 4, and (3) fitting 30-min spectral estimates to an equation for the Kaimal spectral shape. These methods are discussed in more detail in paragraphs below.

Integral time scales were calculated by integrating the autocorrelation function of 10-minute periods of sonic-anemometer-measured streamwise velocity. The mean streamwise velocity was removed before calculating the autocorrelation function, and the function was integrated from 0 lag up to the first zero crossing. This method was also tried for 30-minute records, with much less success. The 30-minute time series (with the 30-min mean removed) gave “reasonable” results only for records where each of the three consecutive 10-minute records that made up the 30-minute record had nearly identical τ values. As a test, autocorrelation functions of individual 10-min periods of streamwise velocity were also calculated and then integrated over all positive lags to estimate τ , rather than to the first zero crossing. This method estimated unrealistically huge integral scales for the unfiltered data. For the data with 10-min means removed, this method estimated τ to be zero, the theoretical expectation for filtered data (see Kaimal and Finnigan, 1994, pages 276-279). Using this technique with 30-min periods produced similar results. This test provided confidence in the calculation method, but was not helpful in estimating τ .

For the spectral-peak method, logarithmic spectra were computed for the time series. The log of the frequencies and the log of the spectrum curves $[fS(f)]$ were fit to a Chebyshev

polynomial. For each fitted curve, the frequency at which the peak occurred was calculated and used to estimate the integral scale, based on a form of Kaimal spectrum commonly used in wind engineering (IEC 61400-1 2005). This spectrum is expressed as

$$\frac{fS(f)}{\sigma^2} = \frac{4fL/U}{(1+6fL/U)^{5/3}}$$

where f is the frequency, L is the Eulerian integral length scale, σ is the standard deviation of wind speed U , and S is the longitudinal power spectral density. Using calculus, it can be shown that the peak of the function $fS(f)$ occurs at $f = U/4L$.

In the Kaimal-spectrum fit method, again logarithmic spectra were computed for the time series using 30-minute records. A line search iteration scheme (similar to Newton's Method) was used to find the length scale that minimized the error between the Kaimal and the computed spectrum. This technique does not always converge for spectra that differ from the Kaimal formulation, and can result in huge values for length scales.

The three calculation methods produced time series with similar trends. The periods where they differ significantly tend to be active periods in which the time series were not stationary. The results shown in this paper are those from the more direct method of integrating the autocorrelation function.

The integral time scale calculations are based on 732 ten-min records (218 thirty-min records) of streamwise velocity measured at each of the 4 sonic anemometers from 0000 to 1200 UTC on the nights of 1-16 September. For the 10-min calculations, there were 67 records on 5 Sept, 70 records on 9 Sept, and 63 records on 15 Sept. For the 30-min calculations, there were 22, 23, and 21 records on the three nights, respectively. The integral time scales from the long-term record were estimated using the spectral-peak method. The period of the spectral peak of

each 30-min record was calculated and divided by 4 to estimate τ (assuming a Kaimal spectral shape). The 30-min records for this dataset were formed by concatenating three consecutive 10-min records that had similar standard deviations (± 0.25 m/s) and had local z/L between -1 and +1. This filtering was done to get spectra that were well-behaved, so that we could model them in one of our turbulence-simulation numerical codes (called *TurbSim*). In this way we obtained 3633 records at 54 m, 2995 records at 67 m, 2158 records at 85 m, and 1152 records at the 116 m level. The measurements were collected between March 13, 2002 and March 28, 2003 and again between August 28, 2003 and September 16, 2003.

REFERENCES

Banta, R.M., 2008: Stable boundary layer regimes from the perspective of the low-level jet.

Acta Geophysica, **56**, 58-87.

Banta, R.M., R.K. Newsom, J.K. Lundquist, Y.L. Pichugina, R.L. Coulter, and L. Mahrt, 2002:

Nocturnal low-level jet characteristics over Kansas during CASES-99. *Boundary-Layer Meteorol.*, **105**, 221-252.

_____, Y.L. Pichugina, and R.K. Newsom, 2003: Relationship between low-level jet properties and turbulence kinetic energy in the nocturnal stable boundary layer. *J. Atmos. Sci.*, **60**, 2549-2555.

_____, Y.L. Pichugina, and W.A. Brewer, 2006: Turbulent velocity-variance profiles in the stable boundary layer generated by a nocturnal low-level jet. *J. Atmos. Sci.*, **62**, 2700-2719.

_____, L. Mahrt, D. Vickers, J. Sun, B. Balsley, Y. Pichugina, and E. Williams, 2007: The very stable boundary layer on nights with weak low-level jets. *J. Atmos. Sci.*, in press.

Blumen, W., R.M. Banta, S.P. Burns, D.C. Fritts, R. Newsom, G.S. Poulos, and J. Sun, 2001: Turbulence statistics of a Kelvin-Helmholtz billow event observed in the nighttime boundary layer during the CASES-99 field program. *Dynamics of Atmos. and Oceans*, **34**, 189-204.

Browning, K. A. and Wexler, R.: 1968, The Determination of Kinematic Properties of a Wind Field Using Doppler Radar. *J. Appl. Meteor.* **7**, 105-113.

Davies, F., C.G. Collier, G.N. Pearson, and K.E. Bozier, 2004: Doppler lidar measurements of turbulent structure function over an urban area. *J. Atmos. Oceanic. Technol.*, **21**, 753-761.

Drobinski P., Dabas, A.M., and P.H. Flamant, 2000: Remote measurement of turbulent wind spectra by heterodyne Doppler lidar technique. *J. Appl. Meteor.* **39**, 2434-2451.

_____, P. Carlotti, R.K. Newsom, R.M. Banta, R.C. Foster and J.L. Redelsperger. 2004: The structure of the near-neutral atmospheric surface layer. *J. Atmos. Sci.* **61**, 699–714.

Eberhard, W.L., R.E. Cupp and K.R. Healy. 1989: Doppler lidar measurement of profiles of turbulence and momentum flux. *J. Atmos. Oceanic Technol.*, **6**, 809–819.

Eckman, R.M., 2008: Comment on “Dynamical implications of block averaging” by G. Treviño and E.L. Andreas. *Bound.-Layer Meteor.*, in press.

Emeis, S., Chr. Münkler, S. Vogt, W.J. Müller, K. Schäfer, 2004: Atmospheric boundary-layer structure from simultaneous SODAR, RASS, and ceilometer measurements. *Atmos. Environ.*, **38**, 273-286.

Gal-Chen, T.M. Xu, and W.L.Eberhard, 1992, Estimates of atmospheric boundary layer fluxes and other turbulence parameters from Doppler lidar data. *J. Geophys. Res.*, **97**, 18,409-18,423

Grund, C. J., R. M. Banta, J. L. George, J. N. Howell, M. J. Post, R. A. Richter, A. M.

Weickmann, 2001: High-resolution Doppler lidar for boundary layer and cloud research. *J. Atmos. Oceanic Technol.*, **18**, 376-393.

Frehlich R., 2001: Estimation of velocity error for Doppler lidar measurements. *J. Atmos. Oceanic Technol.*, **18**, 1628–1639.

_____, 2004: Velocity error for coherent Doppler lidar with pulse accumulation. *J. Atmos. Oceanic Technol.*, **21**, 905–920.

_____, S.M. Hannon, and S.W., Henderson, 1998: Coherent Doppler lidar measurements of wind field statistics. *Boundary-Layer Meteor.*, **86**, 233-256.

Frisch, S., B.W. Orr, and B.E. Martner, 1992: Doppler radar observations of the development of a boundary-layer nocturnal jet. *Mon. Wea. Rev.*, **120**, 3-16.

IEC 61400-1, 2005. Wind turbines-Part 1: Design requirements, 3rd Edition. International Electrotechnical Commission.

J.C. Kaimal and J.J. Finnigan, 1994: *Atmospheric Boundary Layer Flows: Their Structure and Measurement*. Oxford University Press, New York, 289 pp .

Kelley, N, M. Shirazi, D. Jager, S. Wilde, J. Adams, M. Buhl, P. Sullivan, and E Patton, 2004: Lamar Low-Level Jet Project Interim Report. NREL/TP-500-34593. Golden, CO: National Renewable Energy Laboratory.

_____, B.J. Jonkman, G.N. Scott, Y.L. Pichugina, 2007: Comparising Pulsed Doppler Lidar with Sodar and Direct Measurements for Wind Assessment. NREL/CP-500-41792, Golden, CO: National Renewable Energy Laboratory.

Kropfli, R.A., 1986: Single Doppler radar measurements of turbulence profiles in the convective boundary layer. *J. Atmos. Oceanic Technol.*, **3**, 305–314.

Lenschow D.H., J. Mann, and L. Kristensen, 1994: How long is long enough when measuring fluxes and other turbulence statistics. *J. Atmos. Oceanic Technol.*, **11**, 661–673.

_____, V. Wulfmeyer, and C. Senff, 2000. Measuring second- through fourth-order moments in noisy data. *J. Atmos. Oceanic Technol.*, **17**, 1330–1347.

Lothon, M., D.H. Lenschow, and S.D. Mayor, 2006: Coherence and scale of vertical velocity in the connective boundary layer from a Doppler lidar. *Boundary-Layer Meteorol.*, **121**, 521-536.

Mahrt, L., and D. Vickers, 2002: Contrasting vertical structures of nocturnal boundary layers. *Bound.-Layer Meteor.*, **105**, 351-363.

_____, and _____, 2006: Extremely weak mixing in stable conditions. *Bound.-Layer Meteor.*, **119**, 19-39.

Maughan, R.A., Spanton, A.M., Williams, M.L., 1982. An analysis of the frequency distribution of SODAR derived mixing heights classified by atmospheric stability. *Atmosph. Environ.*, **16**, 1209–1218.

Mayor, S. D., D. H. Lenschow, R. L. Schwiesow, J. Mann, C. L. Frush, M. K. Simon, 1997: Validation of NCAR 10.6- μm CO₂ Doppler lidar radial velocity measurements and comparison with a 915-MHz profiler. *J. Atmos. Oceanic Technol.*, **14**, 1110-1126.

Newsom, R.K., and R.M. Banta, 2003: Shear-flow instability in the stable nocturnal boundary layer as observed by Doppler lidar during CASES-99. *J. Atmos. Sci.*, **30**, 16-33.

Newsom R. K. and R.M. Banta. 2004: Assimilating coherent Doppler lidar measurements into a model of the atmospheric boundary layer. Part I: Algorithm development and sensitivity to measurement error. *J. Atmos. Oceanic Technol.*, **21**, 1328–1345.

Panofsky, H. A. and J. A. Dutton, 1984: *Atmospheric Turbulence - Models and Methods for Engineering Applications*. John Wiley and Sons, New York, 397 pp.

Poulos, G.S., W. Blumen, D.C. Fritts, J.K. Lundquist, J. Sun, S. Burns, C. Nappo, R.M. Banta, R.K. Newsom, J. Cuxart, E. Terradellas, B. Balsley, M. Jensen, 2002: CASES-99: A comprehensive investigation of the stable nocturnal boundary layer. *Bull. Amer. Meteor. Soc.*, **83**, 555-581.

Pichugina, Y.L., R. M. Banta, N. D. Kelley, S.P. Sandberg, J. L. Machol, and W. A. Brewer, 2004: Nocturnal low-level jet characteristics over southeastern Colorado. *Preprints, 16th Symposium on Boundary Layers and Turbulence*, paper 4.11, Portland ME, 6 pp.

_____, _____, and _____, 2005: Application of high-resolution Doppler lidar data for wind energy assessment. *Preprints, 2nd Symposium on Lidar Atmospheric Applications*, paper 4.6, San Diego CA, 5 pp.

Orr, B.W., 1990: Boundary layer momentum budgets as determined from a single scanning Doppler radar. M.S. Thesis, Dept of Atmospheric Science, Colorado State Univ., Ft. Collins, 116 pp.

Rye, B.J., and R.M. Hardesty, 1993: Discrete spectral peak estimation in incoherent backscatter heterodyne lidar. I. Correlogram accumulation. *IEEE Trans. Geosci. Remote Sens.*, **31**, 28-35.

_____, and _____, 1993: Discrete spectral peak estimation in incoherent backscatter heterodyne lidar. I: Spectral accumulation and the Cramer-Rao Lower Bound. *IEEE Transactions on Geoscience and Remote Sensing*, **31**, 16-27.

Smalikho I., 2003: Techniques of wind vector estimations from data measured with a scanning coherent Doppler lidar. *J. Atmos. Oceanic Technol.*, **20**, 276–291.

_____, F. Köpp and S. Rahm. 2005: Measurement of atmospheric turbulence by 2- μm Doppler lidar. *J. Atmos. Oceanic Technol.*, **22**, 1733–1747.

Treviño, G., and E.L. Andreas, 2006: Dynamic implications of block averaging. *Bound.-Layer Meteor.*, **120**, 497-508.

_____, and _____, 2008: Reply to comment of R.M. Eckman. *Bound.-Layer Meteor.*, in press.

Vickers, D. and L. Mahrt, 2003: The cospectral gap and turbulent flux calculations. *J. Atmos. Ocean. Technol.*, **20**, 660-672.

_____, and _____, 2006: A solution for flux contamination by mesoscale motions with very weak turbulence. *Bound.-Layer Meteor.*, **118**, 431-447.

Wilson, D.A., 1970: Doppler radar studies of boundary layer wind profiles and turbulence in snow conditions. *Proc., 14th conf. on Radar Meteor.*, Tucson, Amer. Meteor Soc., pp.191-196.

Wulfmeyer, V., M. Randall, W.A. Brewer, and R.M. Hardesty, 2000, 2-mm Doppler lidar transmitter with high frequency stability and low chirp. *Opt. Lett.*, **25**, 1228-1230.

FIGURE CAPTIONS

Figure 1. Vertical-slice scans taken during the night of 9 September from 0315 to 0339 UTC, illustrating the binning procedure. Vertical axis is height (z , km), horizontal axis is distance from the HRDL position at (0.0). All scans shown in the figure were performed at 340° azimuth angle by sweeping in elevation angle from 0 to 20° . The time to perform each scan was about 20 s. Means and variances were calculated over data within a horizontal bin (Δz) and assigned the height of the midpoint of the bin to form a vertical profile. Width of the bin depicted here is 100 m for illustration, but actual intervals used for computing U and σ_u^2 were 1-, 5-, and 10-m.

Figure 2. Profiles of instrument noise, atmospheric and total variances estimated from HRDL starting “scan” performed at fixed 10° azimuth and 10° elevation angles during the night of September 9, 1030-1035 UTC. Figure illustrates an instrument error of less than $0.05 \text{ m}^2 \text{ s}^{-2}$ up to 1100 m.

Figure 3. Scatter plot of TKE and streamwise variance ($\text{m}^2 \text{ s}^{-2}$) measured by sonic anemometers at four tower levels (shown by different colors) during the night of September 15. Data were averaged over 5-min. The best-fit linear regression is shown by solid line.

Figure 4. (a) Profiles of 10-min lidar streamwise velocity (blue) and 10-min sodar wind speed profiles (red), for every hour from 0130 to 0930 UTC during the night of September 15. Red dots show all available sodar data, red pluses are represent sodar data obtained with confidence factor 3 or more. The range of the wind speed within each time interval is $5\text{-}20 \text{ m s}^{-1}$. (b) Scatter plot of data as in (a) obtained for 11 hours during the night. The middle line in the plot represents the best-

fit linear regression and the upper and lower lines are for ± 1 standard deviation. Correlation coefficient and regression parameters in Table 2 were computed only for sodar measurements with confidence factor of 3 or more, which are shown by larger plus signs on the plot.

Figure 5. Time-height cross sections of HRDL streamwise velocity for the night of September 5 (top panel). Each vertical line represents a vertical profile of the wind horizontally averaged within 1-m bins. The vertical axis shows the height AGL. Dotted lines indicate tower levels of 54-, 67-, 85-, and 116-m. The bottom panel shows time-series of sonic (solid line) and lidar (+) data retrieved at the heights of sonic measurements, although the lidar data are mostly hidden by the tower data. The vertical axis shows the wind speed (m s^{-1}), and the horizontal axes of both plots show time in UTC.

Figure 6. Scatter plot of wind speed from sonic anemometers at four tower levels and HRDL-measured streamwise velocity ($U_H, \text{m s}^{-1}$) computed at heights of sonic measurements for the night of September 5. (a) data from both instruments were averaged over 1-min and streamwise velocities were computed within 1-m vertical bins; (b) data averaged over 10-min and streamwise velocities were computed within 10-m vertical bins. The solid line in both plots represents the best-fit linear regression.

Figure 7. Sample profiles of 5 min streamwise (a) velocity (m s^{-1}) and (b) variance ($\text{m}^2 \text{s}^{-2}$) calculated by averaging HRDL vertical-slice scan data within 1-, 5-, and 10- m vertical bins. Figure illustrates the sensitivity of variance to the size of the vertical averaging bin. Profile is from 15 September at 0400 UTC.

Figure 8. Time-height cross sections of HRDL streamwise velocity variance are shown for the night of September 5. Each vertical line represents a variance profile of the streamwise velocity horizontally averaged over 1-min (a) within 1-m bins and (b) within 10-m bins. Color bar indicates magnitude of variance ($\text{m}^2 \text{s}^{-2}$).

Figure 9. (a) Time-height cross sections of HRDL streamwise velocity variance for the night of 15 September 2003 show good agreement in pattern with (b) time series of TKE measured by sonic anemometers at 4 heights and indicated by different colors. Dotted lines in the top panel indicate levels of sonic anemometer measurements at 54-, 67-, 85-, and 116-m AGL.

Figure 10. Scatter plots of sonic-anemometer variance component measured parallel to the lidar scan at four heights, and the streamwise velocity variance, calculated from HRDL vertical slice scans at the same heights, for the night of 15 September 2003. Data are averaged over (left column) 5- min and (right column) 10- min time intervals. Variances were calculated within vertical bins of (top row) 1-m, (middle row) 5-m, and (bottom row) 10-m. The middle line in all plots represents the best-fit linear regression and the upper and lower lines are for ± 1 standard deviation.

Figure 11. Scatter plots of sonic-anemometer-measured TKE at four heights, and streamwise velocity variance at the same heights, computed from HRDL vertical slice scans by averaging data within 1 m vertical bins. Data from both instruments were first averaged over 1-min interval and then again averaged over (a) 3 min, (b) 5 min, (c) 10 min, and (d) 15 min. The middle line in all

plots represents the best-fit linear regression and the upper and lower lines are for ± 1 standard deviation. Data are from the night of 15 September 2003.

Figure A1: Integral time scale τ data calculated for the night of 9 September 2003. a) Time series of τ . b) Histogram of τ distribution for 9 September. c) Histogram for nights during the period of 1-16 September 2003. d) Histogram for all nights of Lamar tower operation (March 2002—March 2003 and 28 August-16 September 2003).

Figure A2: Scatter plots for 0300-0400 UTC the night of 15 September 2003, a period when τ was relatively steady at ~ 4 -5 s. Plots show sonic-anemometer-measured TKE at four heights, and streamwise velocity variance at the same heights, computed from HRDL vertical slice scans by averaging data within 1 m vertical bins. Data from both instruments were first averaged over 1-min interval and then again averaged over (a) 3 min, (b) 5 min, (c) 10 min, and (d) 15 min. The middle line in all plots represents the best-fit linear regression and the upper and lower lines are for ± 1 standard deviation.

Table 1: Parameters of linear regression between data measured by lidar, sodar and sonic anemometers.

Table 2. Correlation coefficients r between the sonic-anemometer mean-wind speed at four tower levels and the mean streamwise velocity, computed from HRDL vertical-slice scans, evaluated at the same level as the tower data.

Table A1. Estimated Eulerian integral time scales in seconds. Values were calculated using three methods, including (1) Lag Method: integrating the 10-min autocorrelation function of the streamwise fluctuating velocity signal, (2) Spectral Peak Method: dividing the period of the 30-min spectral peak, $fS(f)$, by 4, and (3) Kaimal Spectra Method: fitting 30-min spectral estimates to an equation for the Kaimal spectral shape.

Table 1. Parameters of linear regression between data measured by lidar, sodar and sonic anemometers.

Variables	Averaging intervals	Figure	N	Bias (m s ⁻¹)	Slope	R
$U_{SODAR} - U_H$	10m, 10min	4b	948	0.836±0.460	1.058±0.032	0.94
$U_{SONIC} - U_H$	1m, 1min	6a	1593	0.64±0.29	1.006±0.029	0.95
$U_{SONIC} - U_H$	10m, 10min	6b	204	0.64±0.31	1.006±0.080	0.98
				(m ² s ²)		
$\sigma^2_{SONIC} - TKE_{SONIC}$	5min	3	700	0.003± 0.008	1.053± 0.033	0.98
$\sigma^2_{SONIC} - \sigma^2_H$	1m, 1min	-	1527	-0.032±0.018	0.770 ±0.042	0.74
	1m, 5min	10a	355	-0.025±0.024	0.990 ±0.032	0.85
	1m,10min	10b	187	-0.017±0.040	0.988 ±0.048	0.83
	5m, 1min	-	1523	-0.041±0.019	0.770 ±0.042	0.74
	5m, 5min	10c	351	-0.023±0.025	0.967 ±0.032	0.85
	5m, 10min	10d	183	-0.181±0.052	1.010 ±0.055	0.82
	10m, 1min	-	1532	-0.080±0.020	0.694±0.038	0.73
	10m, 5min	10e	352	-0.127±0.029	0.955 ±0.033	0.84
	10m, 10min	10f	183	-0.132±0.051	0.973 ±0.052	0.81
$TKE_{SONIC} - \sigma^2_U$	1m, 1min	-	1527	-0.037±0.018	0.815 ±0.044	0.76
	1m, 5min	-	355	-0.030±0.025	0.889 ±0.033	0.82
	1m,10min	-	187	-0.021±0.040	0.867 ±0.047	0.81
	5m, 1min	-	1523	-0.048±0.019	0.819 ±0.043	0.76
	5m, 5min	-	351	-0.029±0.024	0.950 ±0.031	0.85
	5m, 10min	-	183	-0.166±0.050	0.941 ±0.052	0.80
	10m, 1min	-	1532	-0.089±0.020	0.737±0.368	0.75
	10m, 5min	-	352	-0.126±0.029	0.934 ±0.032	0.83
	10m, 10min	-	183	-0.126±0.048	0.913 ±0.050	0.81
$TKE_{SONIC} - \sigma^2_U$	1m, 1min over 3min	11a	640	0.008 ±0.013	0.940 ±0.020	0.88
	1m, 1min over 5min	11b	384	-0.001 ±0.017	0.959 ±0.027	0.88
	1m, 1min over 10min	11c	192	-0.044 ±0.023	1.023 ±0.036	0.90
	1m, 1min over 15min	11d	1527	-0.078 ±0.028	1.074 ±0.041	0.92

Table 2. Coefficients of correlation between the wind speed, measured by sonic anemometers at 4 tower levels during LLLJP experiment, and mean streamwise velocity, computed from HRDL vertical-slice scans.

day	54 m	67 m	85 m	116 m	Mean
02	0.93	0.87	0.82	0.84	0.87
03	0.73	0.71	0.69	0.70	0.71
05	0.96	0.95	0.95	0.95	0.95
06	0.90	0.90	0.90	0.93	0.91
09	0.91	0.93	0.93	0.94	0.93
10	0.92	0.93	0.93	0.93	0.93
11	0.76	0.76	0.73	0.80	0.76
12	0.70	0.72	0.79	0.76	0.74
13	0.79	0.78	0.80	0.79	0.79
15	0.95	0.94	0.95	0.95	0.95
16	0.84	0.81	0.80	0.84	0.83

Table A1. Estimated Eulerian integral time scales in seconds. Values shown were calculated using 3 methods, including (1) Lag Method: integrating the 10-min autocorrelation function of the streamwise fluctuating velocity signal, (2) Spectral Peak Method: dividing the period of the 30-min spectral peak, $fS(f)$, by 4, and (3) Kaimal Spectra Method: fitting 30-min spectral estimates to an equation for the Kaimal spectral shape.

	54 m			67 m			85 m			116 m		
	Mode	Median	Mean	Mode	Median	Mean	Mode	Median	Mean	Mode	Median	Mean
Lag Method (10 min)												
September 5	4	10	16	4	12	17	3	11	20	2	20	27
September 9	4	10	16	3	9	17	3	15	21	4	25	32
September 15	3	8	14	4	6	15	4	9	17	4	16	23
September 1-16	5	13	22	5	15	24	5	20	28	4	31	35
Spectral Peak Method												
September 5	5	5	7	4	5	29	4	6	20	5	10	63
September 9	4	5	27	4	5	37	3	7	69	2	12	112
September 15	4	5	18	3	4	17	3	3	29	2	5	40
September 1-16	4	8	43	4	8	50	4	10	73	5	16	105
March 2002- September 2003	5	6	10	5	6	11	5	6	12	5	7	16
Kaimal Spectra Method												
September 5	9	10	87	5	10	102	5	14	97	7	18	184
September 9	5	9	35	4	10	40	4	11	57	4	41	168
September 15	4	7	50	4	7	87	5	7	180	8	7	265
September 1-16	6	14	114	10	17	151	5	22	298	8	52	655

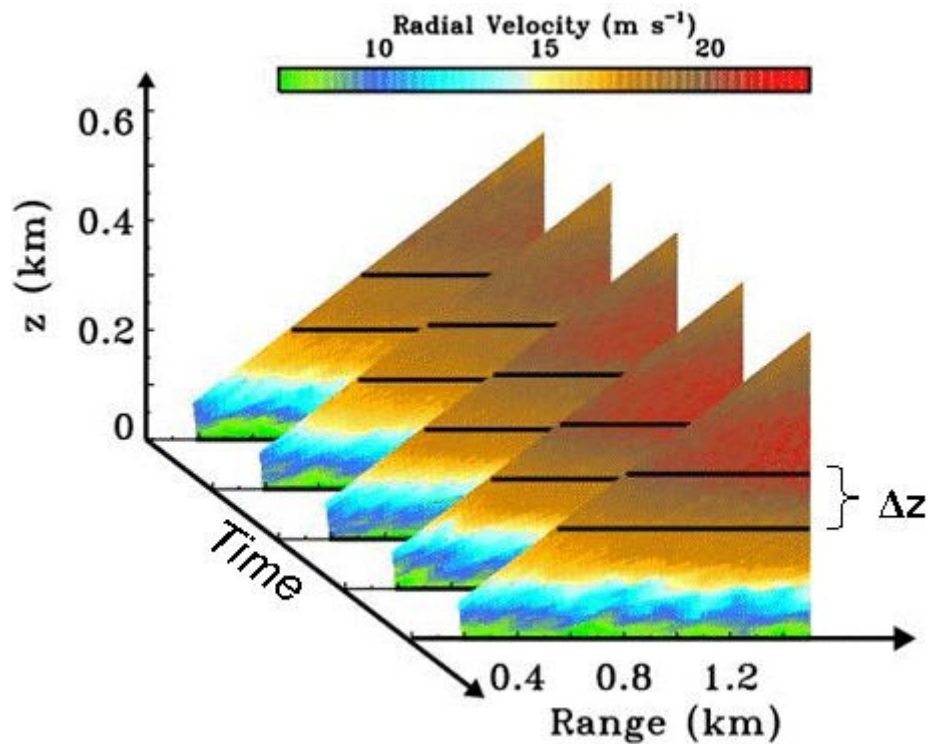


Figure 1. Vertical-slice scans taken during the night of 9 September from 0315 to 0339 UTC, illustrating the binning procedure. Vertical axis is height (z , km), horizontal axis is distance from the HRDL position at (0.0). All scans shown in the figure were performed at 340° azimuth angle by sweeping in elevation angle from 0 to 20° . The time to perform each scan was about 20 s. Means and variances were calculated over data within a horizontal bin (Δz) and assigned the height of the midpoint of the bin to form a vertical profile. Width of the bin depicted here is 100 m for illustration, but actual intervals used for computing U and σ_u^2 were 1-, 5-, and 10-m.

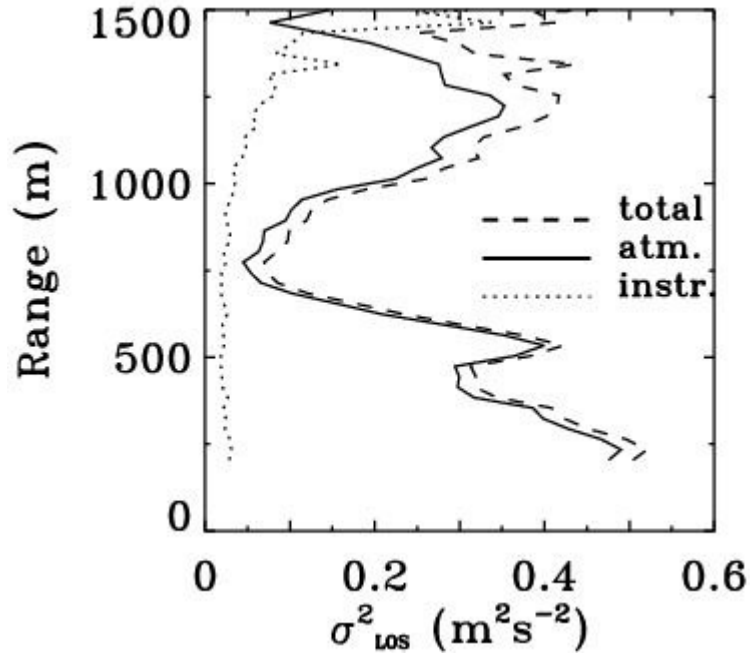


Figure 2. Profiles of instrument noise, atmospheric and total variances estimated from HRDL staring “scan” performed at fixed 10^0 azimuth and 10^0 elevation angles during the night of September 9, 1030-1035 UTC. Figure illustrates an instrument error of less than $0.05 \text{ m}^2 \text{ s}^{-2}$ up to 1100 m.

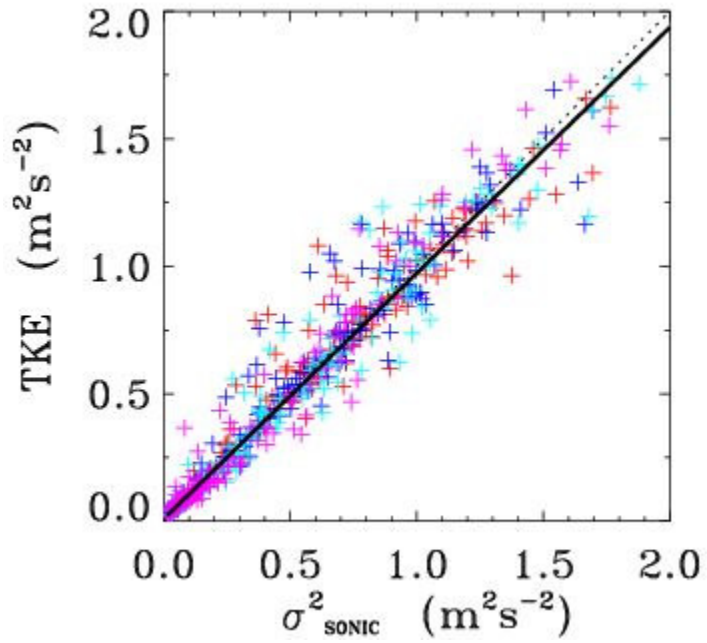


Figure 3. Scatter plot of TKE and streamwise variance ($\text{m}^2 \text{s}^{-2}$) measured by sonic anemometers at four tower levels (shown by different colors) during the night of September 15. Data were averaged over 5-min. The best-fit linear regression is shown by solid line.

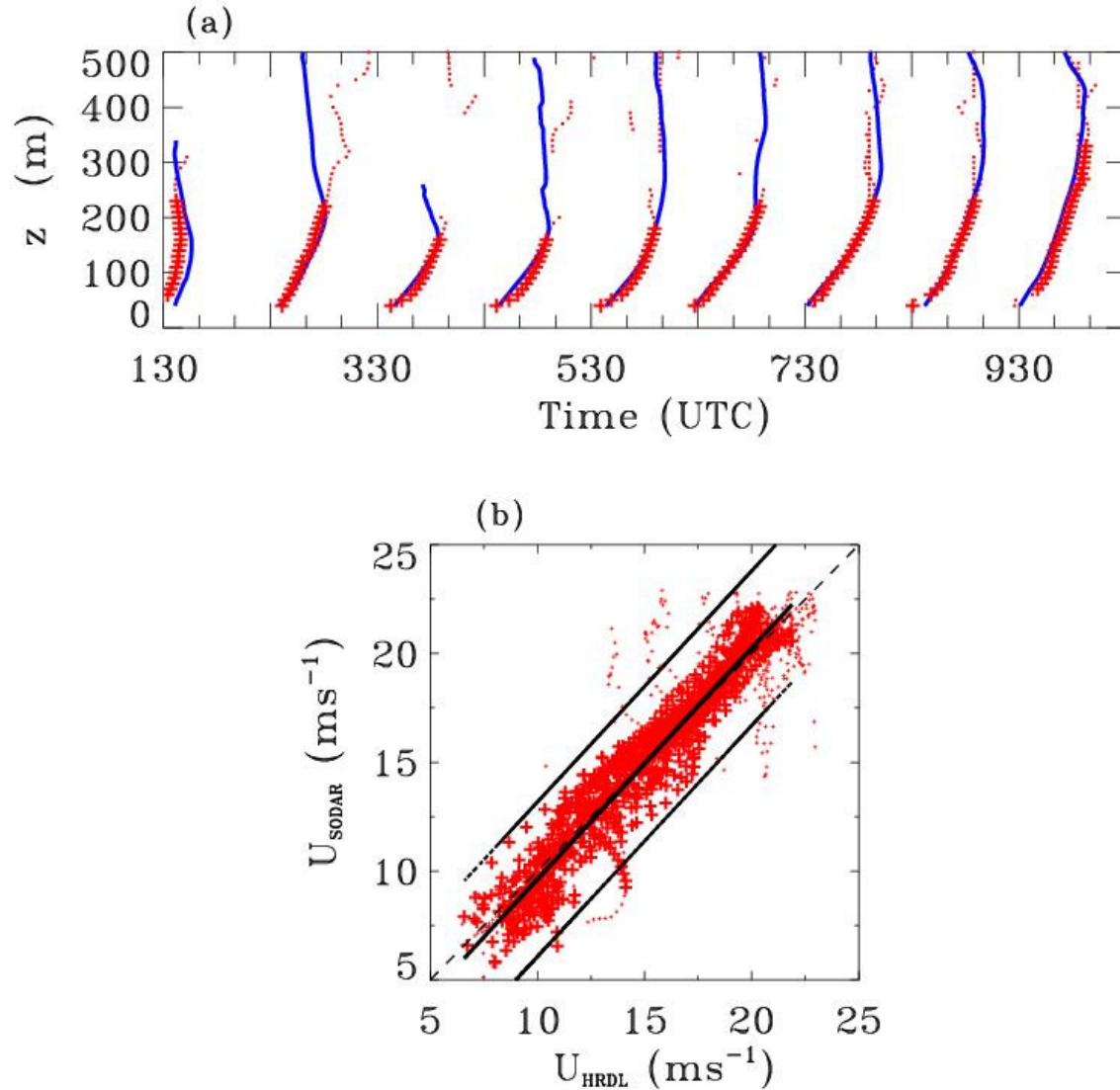


Figure 4. (a) Profiles of 10-min lidar streamwise velocity (blue) and 10-min sodar wind speed profiles (red), for every hour from 0130 to 0930 UTC during the night of September 15. Red dots show all available sodar data, red pluses are represent sodar data obtained with confidence factor 3 or more. The range of the wind speed within each time interval is 5-20 m s^{-1} . (b) Scatter plot of data as in (a) obtained for 11 hours during the night. The middle line in the plot represents the best-fit linear regression and the upper and lower lines are for ± 1 standard deviation. Correlation coefficient and regression parameters in Table 2 were computed only for sodar measurements with confidence factor of 3 or more, which are shown by larger plus signs on the plot.

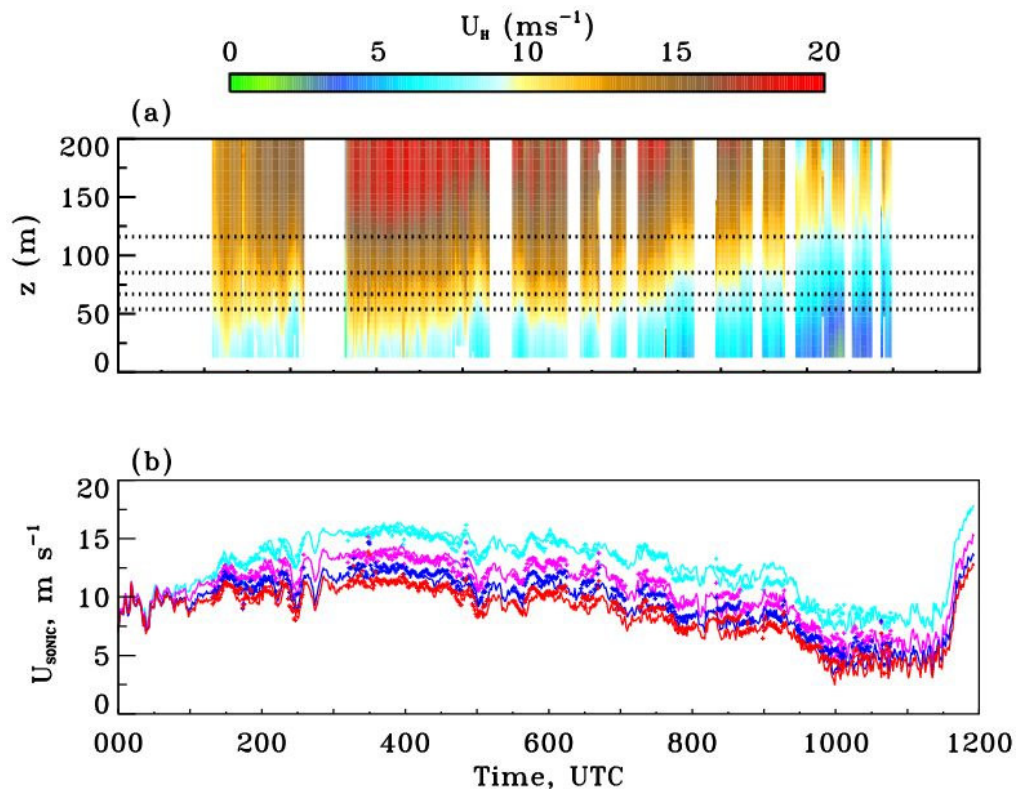


Figure 5. Time-height cross sections of HRDL streamwise velocity for the night of September 5 (top panel). Each vertical line represents a vertical profile of the wind horizontally averaged within 1-m bins. The vertical axis shows the height AGL. Dotted lines indicate tower levels of 54-, 67-, 85-, and 116-m. The bottom panel shows time-series of sonic (solid line) and lidar (+) data retrieved at the heights of sonic measurements, although the lidar data are mostly hidden by the tower data. The vertical axis shows the wind speed (m s^{-1}), and the horizontal axes of both plots show time in UTC.

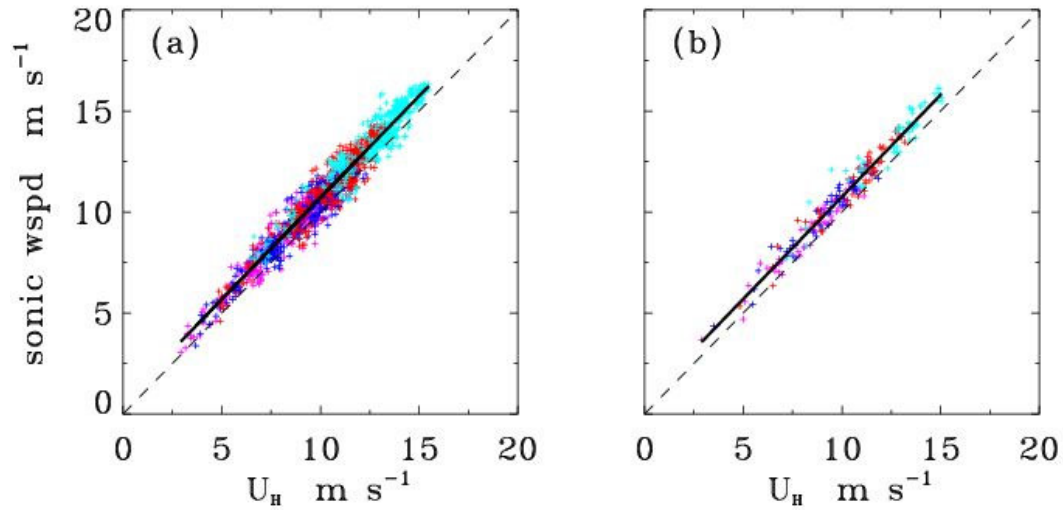


Figure 6. Scatter plot of wind speed from sonic anemometers at four tower levels and HRDL-measured streamwise velocity (U_H , m s^{-1}) computed at heights of sonic measurements for the night of September 5. (a) data from both instruments were averaged over 1-min and streamwise velocities were computed within 1-m vertical bins; (b) data averaged over 10-min and streamwise velocities were computed within 10-m vertical bins. The solid line in both plots represents the best-fit linear regression.

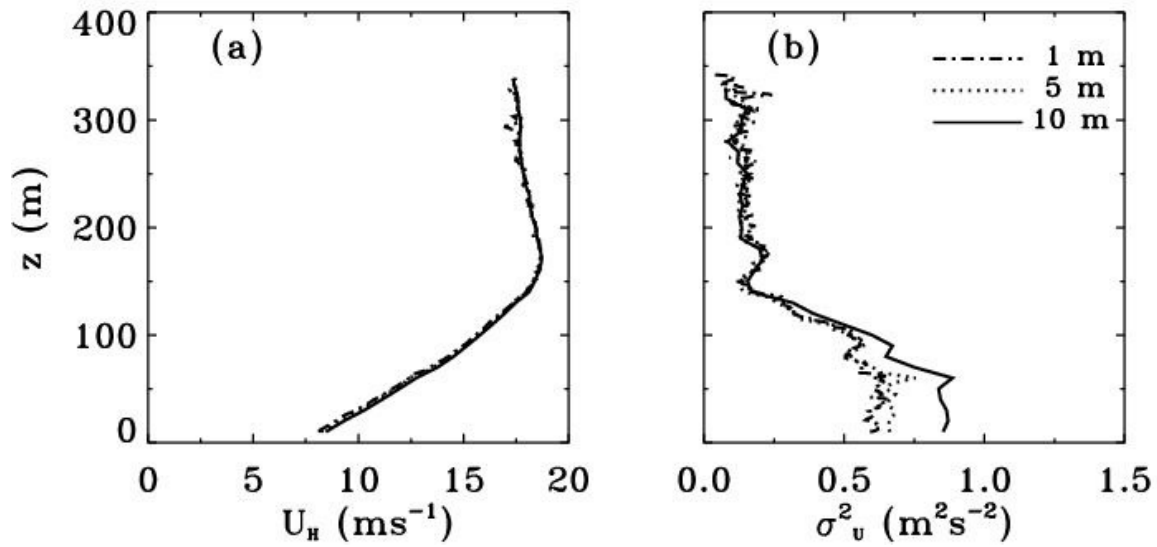


Figure 7. Sample profiles of 5 min streamwise (a) velocity (m s^{-1}) and (b) variance ($\text{m}^2 \text{s}^{-2}$) calculated by averaging HRDL vertical-slice scan data within 1-, 5-, and 10- m vertical bins.

Figure illustrates the sensitivity of variance to the size of the vertical averaging bin. Profile is from 15 September at 0400 UTC.

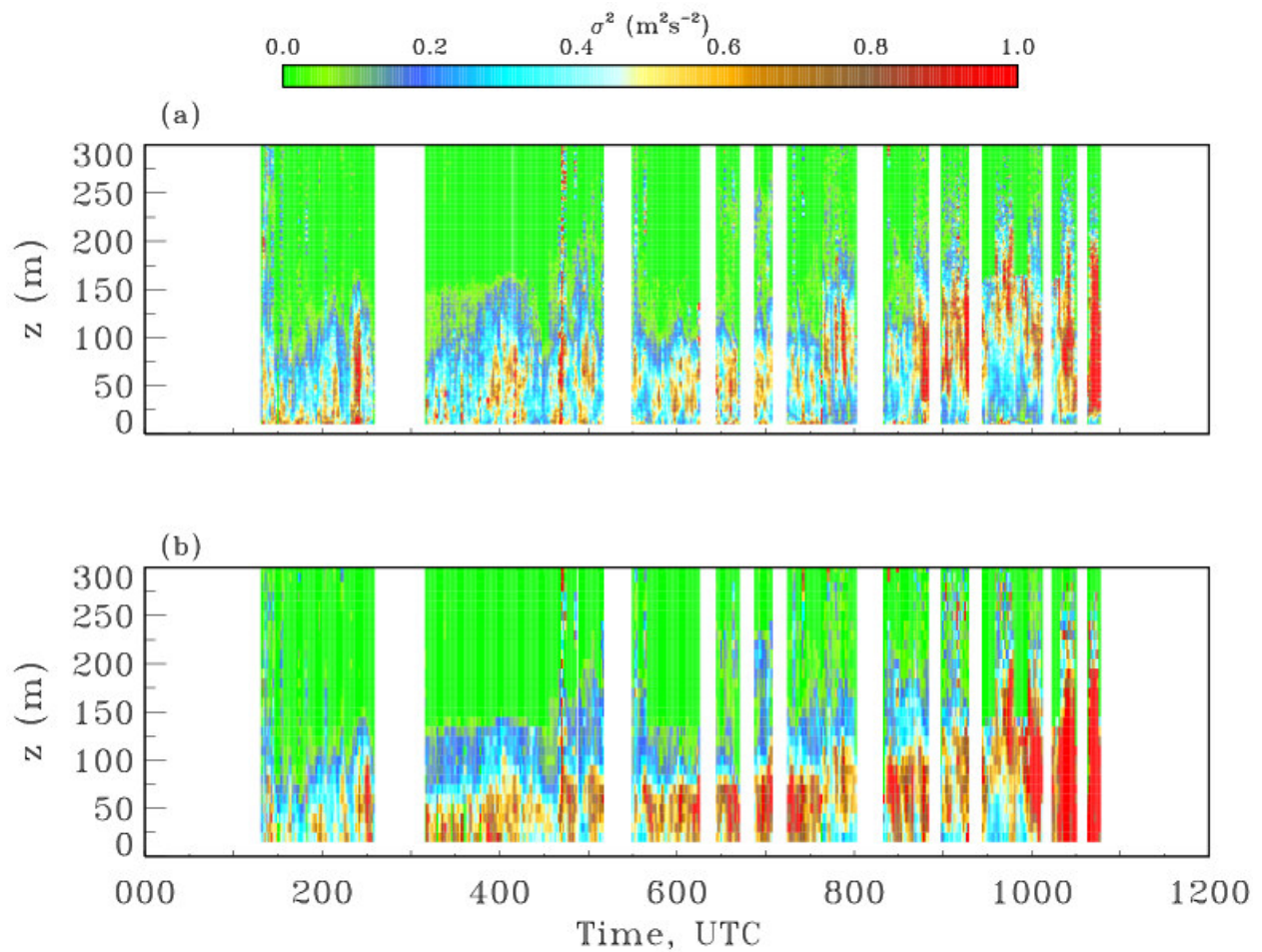


Figure 8. Time-height cross sections of HRDL streamwise velocity variance are shown for the night of September 5. Each vertical line represents a variance profile of the streamwise velocity horizontally averaged over 1-min (a) within 1-m bins and (b) within 10-m bins. Color bar indicates magnitude of variance ($\text{m}^2 \text{s}^{-2}$).

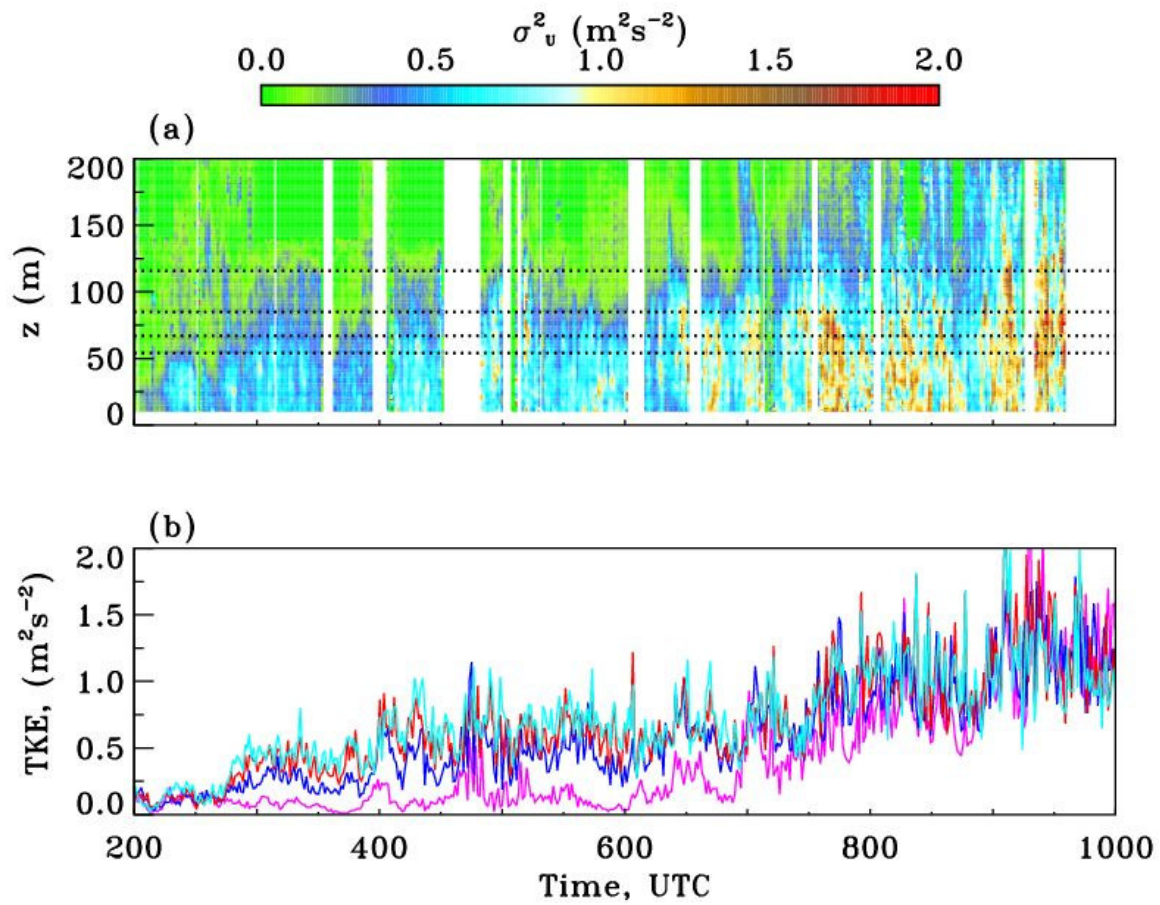


Figure 9. (a) Time-height cross sections of HRDL streamwise velocity variance for the night of 15 September 2003 show good agreement in pattern with (b) time series of TKE measured by sonic anemometers at 4 heights and indicated by different colors. Dotted lines in the top panel indicate levels of sonic anemometer measurements at 54-, 67-, 85-, and 116-m AGL.

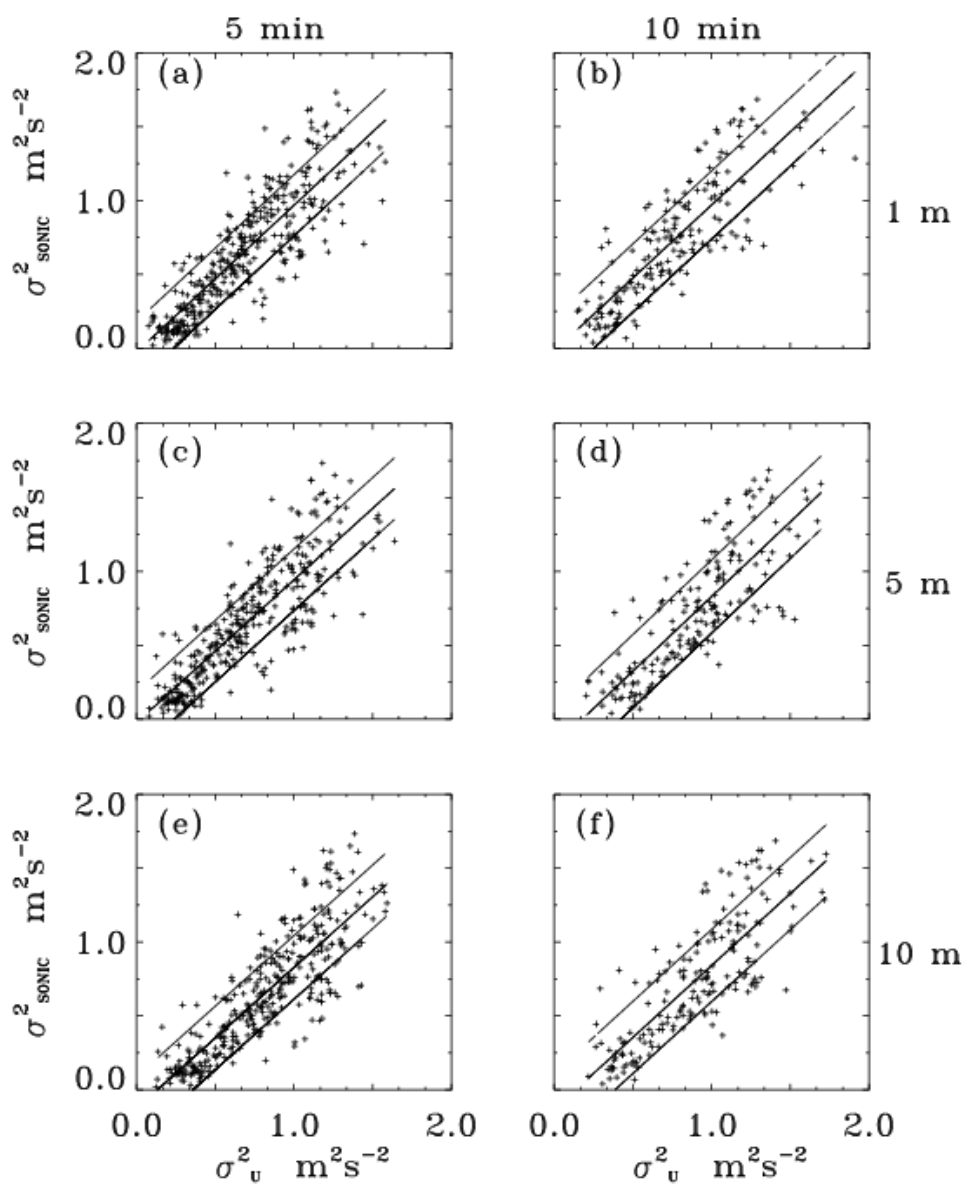


Figure 10. Scatter plots of sonic-anemometer variance component measured parallel to the lidar scan at four heights, and the streamwise velocity variance, calculated from HRDL vertical slice scans at the same heights, for the night of 15 September 2003. Data are averaged over (left column) 5- min and (right column) 10- min time intervals. Variances were calculated within vertical bins of (top row) 1-m, (middle row) 5-m, and (bottom row) 10-m. The middle line in all plots represents the best-fit linear regression and the upper and lower lines are for ± 1 standard deviation.

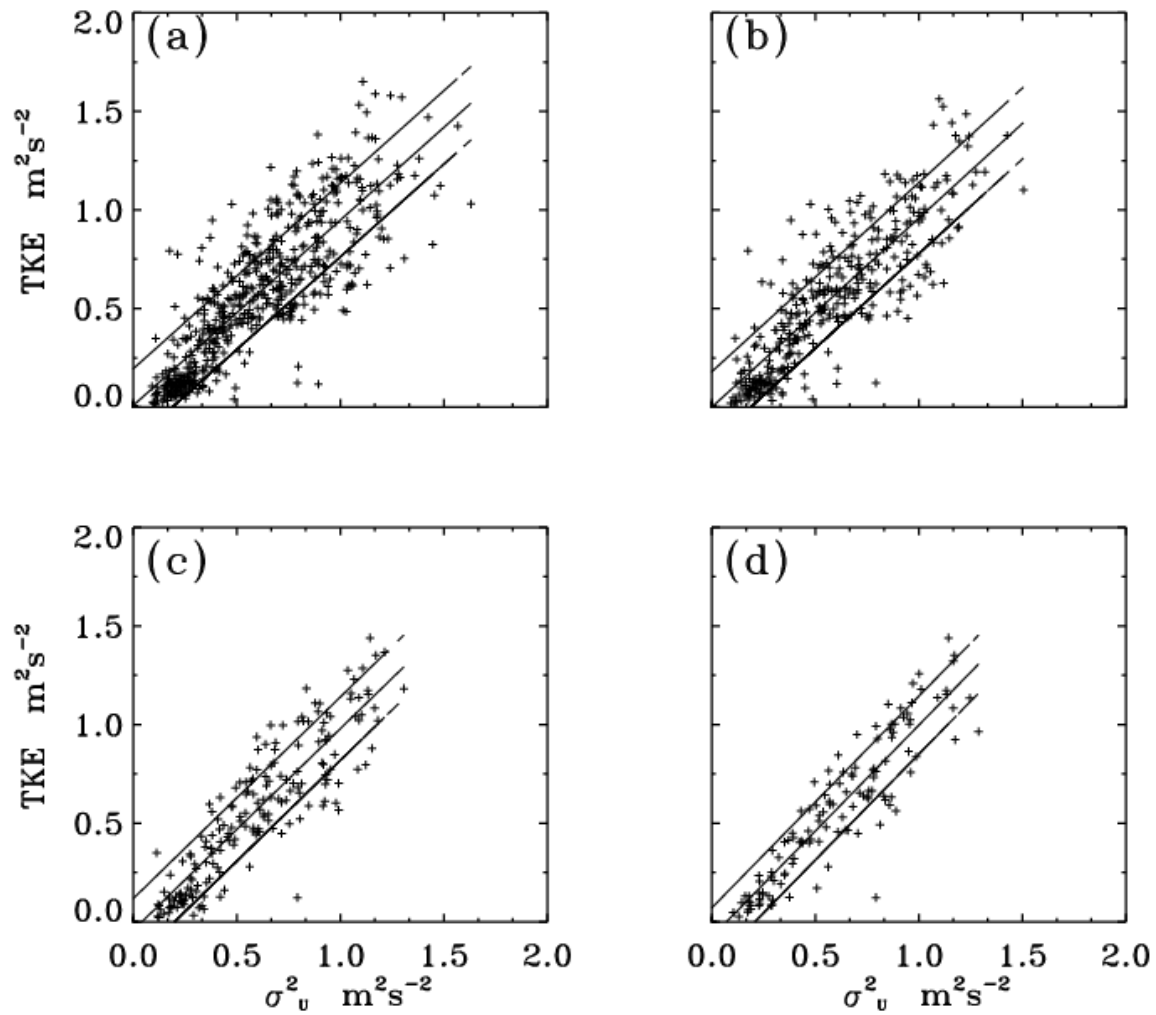


Figure 11. Scatter plots of sonic-anemometer-measured TKE at four heights, and streamwise velocity variance at the same heights, computed from HRDL vertical slice scans by averaging data within 1 m vertical bins. Data from both instruments were first averaged over 1-min interval and then again averaged over (a) 3 min, (b) 5 min, (c) 10 min, and (d) 15 min. The middle line in all plots represents the best-fit linear regression and the upper and lower lines are for ± 1 standard deviation. Data are from the night of 15 September 2003.

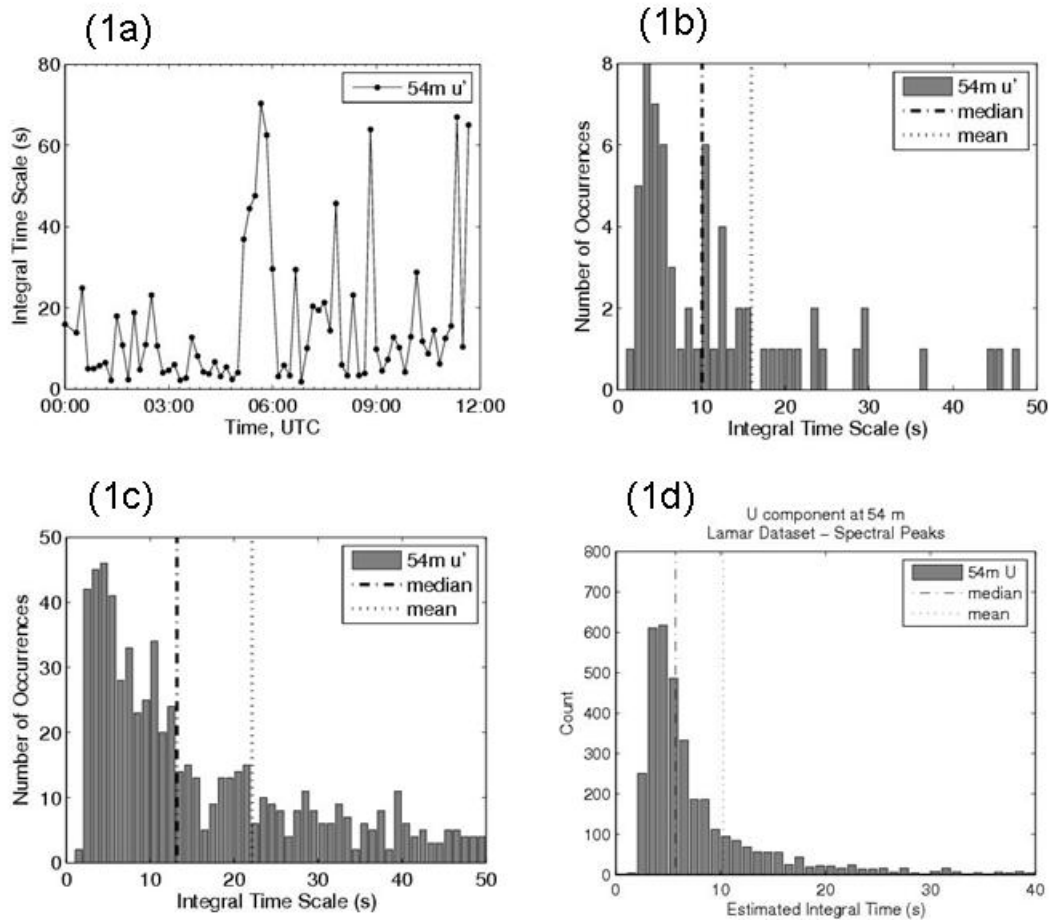


Figure A1: Integral time scale τ data calculated for the night of 9 September 2003. a) Time series of τ . b) Histogram of τ distribution for 9 September. c) Histogram for nights during the period of 1-16 September 2003. d) Histogram for all nights of Lamar tower operation (March 2002—March 2003 and 28 August-16 September 2003).

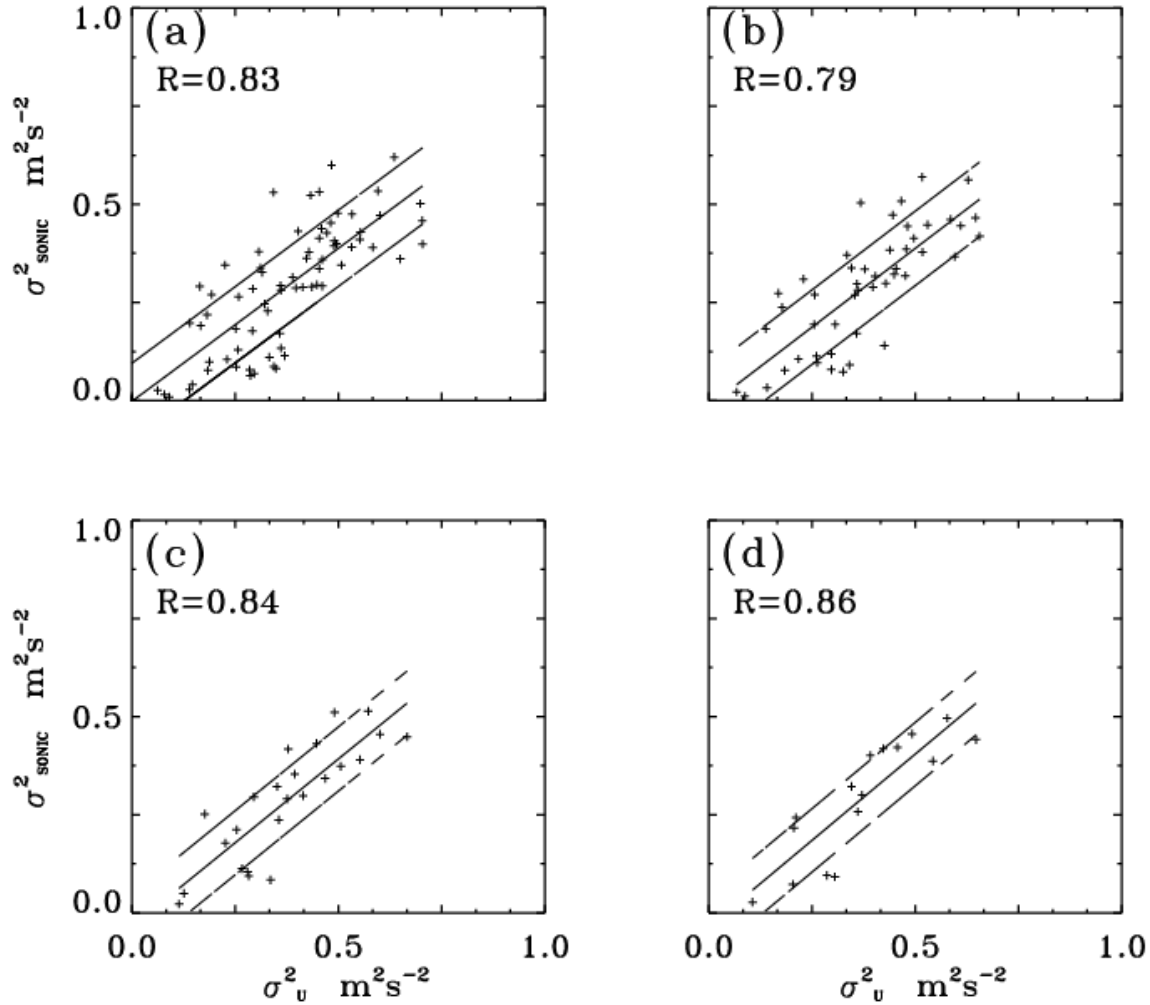


Figure A2: Scatter plots for 0300-0400 UTC the night of 15 September 2003, a period when τ was relatively steady at ~ 4 -5 s. Plots show sonic-anemometer-measured TKE at four heights, and streamwise velocity variance at the same heights, computed from HRDL vertical slice scans by averaging data within 1 m vertical bins. Data from both instruments were first averaged over 1-min interval and then again averaged over (a) 3 min, (b) 5 min, (c) 10 min, and (d) 15 min. The middle line in all plots represents the best-fit linear regression and the upper and lower lines are for ± 1 standard deviation.